Bro1 directly stimulates Vps4 activity to promote Intralumenal Vesicle Formation during Multivesicular Body biogenesis

Authors: *Chun-che Tseng[1,2], *Shirley Dean[1,2,3], *Brian A. Davies[1], Ishara F. Azmi[1,2,4], Natalya Pashkova[5], Johanna A. Payne[1], Jennifer Staffenhagen[6], Matt West[7], Robert C. Piper[5], Greg Odorizzi[7], #David J. Katzmann[1,2]

1) Department of Biochemistry and Molecular Biology, Mayo Clinic, Rochester, MN, 55905
2) Biochemistry and Molecular Biology Graduate Program, Mayo Clinic Graduate School of Biomedical Sciences, Mayo Clinic, Rochester, MN, 55905
3) present address: Adjunct Chemistry Instructor, Cornerstone University, Grand Rapids, MI, 49525
4) present address: CRISPR Therapeutics, 610 Main St. North, Cambridge, MA, 02139
5) Department of Molecular Physiology and Biophysics, Carver College of Medicine, University of Iowa, Iowa City, IA, 52242
6) present address: College of Saint Benedicts, St. Joseph, MN, 56374
7) Department of Molecular, Cellular, and Developmental Biology, University of Colorado – Boulder, Boulder, CO, 80309

*These authors contributed equally to these studies

#To whom correspondence should be addressed

Abstract:
Endosomal sorting complexes required for transport (ESCRT-0, -I, -II, -III) form intralumenal vesicles (ILVs) during the conversion of endosomes to multivesicular bodies (MVBs). The assembly and disassembly of an ESCRT-III polymer facilitates membrane remodeling and scission during this process. The ESCRT-III-associated protein Bro1 (the yeast homolog of mammalian proteins ALIX and HD-PTP) promotes ESCRT-III assembly and inhibits disassembly of ESCRT-III filaments by impeding Vps4, a AAA-ATPase that dismantles ESCRT-III polymers. Here we show that the evolutionarily conserved "V domain" of Bro1-family proteins directly stimulate Vps4 ATPase activity and this activity is enhanced by interaction with ubiquitin. Surprisingly, a carboxyl-terminal fragment of Bro1 containing the V domain supports ILV formation but not sorting of cargo into ILVs, revealing that these two processes can be uncoupled. These studies implicate Bro1 as a factor coordinating cargo sorting with direct regulation of Vps4 to modulate ESCRT-III driven ILV formation during MVB biogenesis.

36 **Introduction:**
37 The Endosomal Sorting Complexes Required for Transport (ESCRTs) are required for
38 multivesicular body (MVB) sorting of ubiquitinated transmembrane protein cargoes [1,2]. There are
39 two well-described functions of the ESCRTs during MVB sorting: 1) recognition of
40 ubiquitinated cargoes via ubiquitin (Ub)-binding domains within ESCRT-0, -I, and -II; and 2)
41 membrane deformation and scission during intralumenal vesicle (ILV) formation, performed by
42 ESCRT-III and associated factors including the AAA-ATPase Vps4 [3-5]. In addition to MVB
43 sorting, ESCRTs have been implicated in other cellular processes including abscission during
44 cytokinesis [6], viral budding [7], extracellular vesicle biogenesis [8], and nuclear pore surveillance [9].
45 All of these events involve membrane remodeling facilitated by ESCRT-III and Vps4; thus, this
46 core process represents the most evolutionarily conserved aspect of ESCRT function [10].
47
48 ESCRT-III subunits are monomeric in the cytosol and undergo ordered polymerization into
49 structures on membranes — thought to be represented by filamentous spirals — that facilitate
50 membrane budding and scission [11-15]. The AAA-ATPase Vps4 disassembles the ESCRT-III
51 polymer, thereby recycling monomeric subunits back into the cytosol [5,16-18], but more recent
52 work has suggested that Vps4 function is required for dynamic exchange of ESCRT-III subunits
53 within filaments during ILV formation prior to their disassembly [19]. The relationship between
54 this ESCRT-III assembly/remodeling/disassembly cycle and ILV formation remains ill-defined,
55 with models ranging from Vps4 merely disassembling ESCRT-III subsequent to vesicle
56 formation (analogous to the role of NSF in SNARE-mediated fusion) [20-22] to a more active role
57 together with ESCRT-III during membrane remodeling and scission [19,23-27]. Insufficient
58 understanding of both the relevant structures and compositions of ESCRT-III, as well as
59 technical limitations, have precluded investigation into the mechanism(s) of ESCRT-III
60 "remodeling" by Vps4, although studies have documented ultrastructural changes in model
61 ESCRT-III polymers upon addition of Vps4 *in vitro* or expression of VPS4 dominant negative *in*
62 *vivo* [20,28-32]. Regardless, a series of regulators, including ESCRT-III itself, the Vps4 cofactor
63 Vta1, and the ESCRT-associated factor Bro1, serve to coordinate the activities of ESCRT-III and
64 Vps4 to optimize ESCRT function during MVB sorting [23,26,33-52].
65
66 Bro1 proteins, including mammalian orthologs HD-PTP and ALIX, possess similar domain
67 architecture — the Bro One Domain (BOD), V domain and Proline Rich Region (PRR) —
68 allowing them to impact ESCRT function through interactions with: Ub/cargo [48,53-56], "early"
69 ESCRT sub-complexes [46,48,57-60], and "late" ESCRT factors including ESCRT-III and de-
70 ubiquitinating enzymes [26,45,49,61-69]. Here we provide evidence that the V domain of Bro1 family
71 members directly modulates Vps4, conferring a level of regulation critical during ILV

biogenesis. We propose this novel mode of regulation is critical for the coordination of ESCRT cargo sorting and ILV formation.

Results:

Separation of cargo sorting and ILV formation during MVB biogenesis

ESCRT-III and Vps4 serve as the core machinery driving a variety of topologically similar membrane remodeling events. Bro1 family members serve critical roles in concert with ESCRTs during MVB sorting, viral budding and cytokinesis. In the contexts of MVB sorting and viral budding, Bro1 family members have been implicated as cargo adaptors capable of supporting cargo recognition through binding Ub-modified cargo or YPxL-motifs within cargo [48,54,65,84,85]. Relevant to the membrane sculpting activity of ESCRTs, the BOD of Bro1 promotes ESCRT-III polymerization through both facilitating Snf7 activation [86] and inhibiting Vps4-mediated disassembly of ESCRT-III [26]. MVB sorting defects upon BOD overexpression [26] suggested this truncation was defective due to loss of function normally provided by the V domain or Proline-Rich Region (PRR). This idea was first tested via morphological analysis of MVBs in WT cells expressing a Bro1 fragment lacking the BOD (a C-terminal fragment containing the V and PRR domains; Figure 1A). Quantitation of ILV budding events revealed a reduction in the surface area of the budding profiles and reduced ILV size, with a trend towards reduced budding intermediates as compared to WT cells (Figure 1B, Figure 1 Supplement 1, Figure 1 Supplement Movies 1, 2). As thisis consistent with accelerated ILV formation resulting from a stimulatory activity within this C-terminal Bro1 fragment, complementation of *bro1*Δ was next examined. While *bro1*Δ cells fail to generate ILVs and displayed multi-lamellar endosomal stacks characteristic of "class E vps" endosomal compartments ([45] and Figure 1C, Figure 1 Supplement Movie 3), cells over-expressing Bro1CTF (aa 370-844) as their sole form of Bro1 displayed spherical endosomal structures containing ILVs (Figure 1C, Figure 1 Supplement Movie 4). While morphologically comparable to WT MVBs, quantitative analyses of the endosomal budding profiles and ILVs indicated that Bro1CTF expression resulted in smaller budding profiles than WT cells, a trend towards reduced numbers of ILV budding intermediates per MVB, and a slight increase in ILV size (Figure 1D, Figure 1 Supplement Movie 4). These results indicate that Bro1CTF is sufficient for ILV formation in the absence of endogenous (full-length) Bro1 and support the interpretation that this fragment enhances ILV budding and/or scission kinetics.

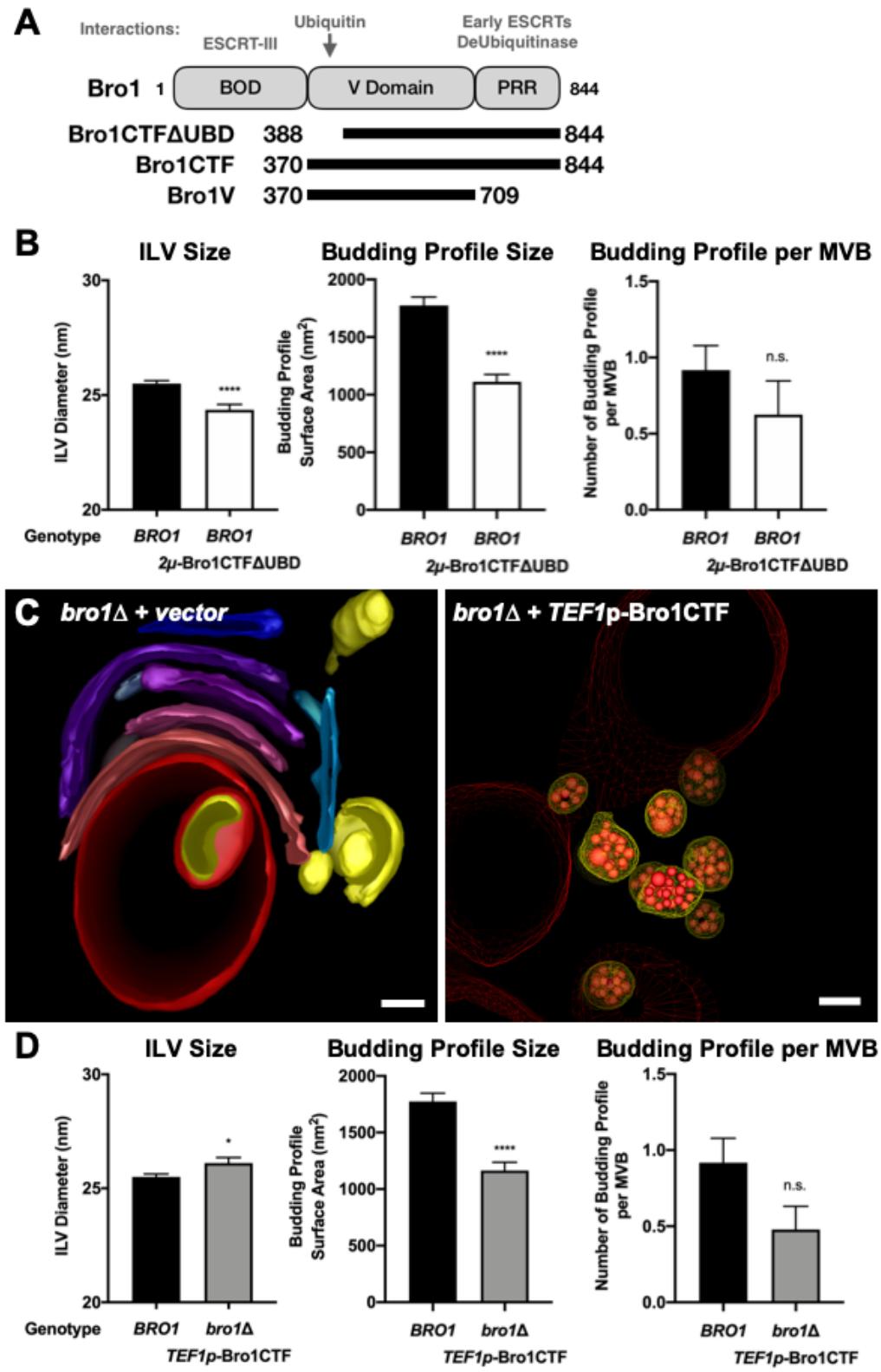

105

106 ***FIGURE 1. C-terminal fragment of Bro1 is sufficient for ILV formation in vivo. (A)*** *Domain*
107 *cartoon of Bro1 (amino acids 1-844).* ***(B)*** *WT (SEY6210) or WT cells overexpressing the C-*

terminal fragment of Bro1 containing the V and PRR domains (Bro1CTFΔUBD) were analyzed by electron tomography for ILV size, the frequency of incomplete ILV budding events per MVB, as well as the average area of those budding events. A minimum of 19 MVBs and 337 ILVs were measured. ***(C)*** *Three-dimensional models reconstructed from 200-nm-thick section electron tomograms of bro1Δ (GOY65) and bro1Δ::TEF1p-Bro1CTF (CTY2) cells. The bro1Δ cells have class E compartments, which are flattened stacks of endosomal membranes that generally lack internal vesicles. Cisternal class E compartment stacks are shown in different colors to differentiate individual membranes. The limiting membrane of the MVB is labeled yellow, and the ILVs are highlighted in red, while the vacuole limiting membrane is labeled as red mesh. Scale bar = 100nm.* ***(D)*** *WT and bro1Δ::TEF1p-Bro1CTF (CTY2) were analyzed by electron tomography for the average ILV size, frequency of incomplete ILV budding events and budding profile area. A minimum of 19 MVBs and 337 ILVs from at least 5 cells were quantified. Error bars indicate mean ± S.E.M. Statistical significances are indicated (n.s., not significant; *, p = 0.0177; ****, p < 0.0001).*

Previous work revealed Bro1 requires interaction of the BOD with Snf7 for MVB cargo sorting [26]; however, we observed ILV formation upon over-expression of Bro1CTF (lacking the BOD). A variety of GFP-tagged MVB cargoes were analyzed to determine whether cargo sorting was supported by Bro1CTF as the sole source of Bro1. In spite of supporting ILV formation, Bro1CTF expressing cells exhibited defects in MVB cargo sorting with cargoes localizing to the limiting membrane of the vacuole and the class E compartment (Figure 2). This analysis included MVB cargoes from the endocytic (Ste2, Mup1) and biosynthetic pathways (Cps1, Ub-Cps1, Cos1, Cos2, Cos5, Sna3) as well as a vacuolar limiting membrane protein, DPAP-B (typically excluded from MVB sorting). The range of cargoes defective for sorting indicate a general defect in MVB protein sorting. The ability of Bro1CTF to support ILV formation without promoting MVB cargo sorting suggested: 1) Bro1CTF is able to activate ESCRT function at the level of ESCRT-III/Vps4 membrane remodeling and scission activity *in vivo*, and 2) this activity is uncoupled from the process of cargo packaging in this context. Moreover, this activity does not depend on the ability Bro1 to interact directly with ESCRT-III via the BOD.

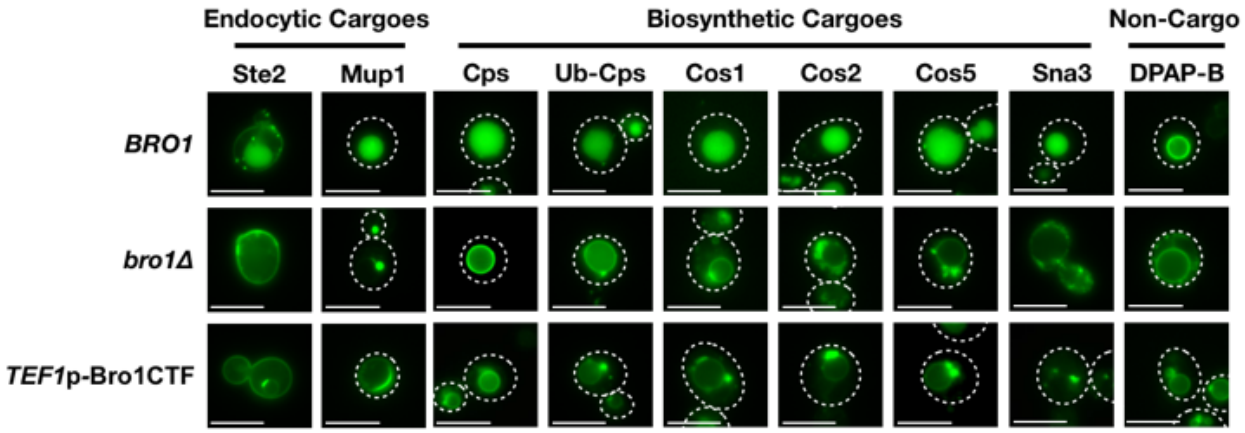

FIGURE 2. Bro1CTF does not rescue MVB cargo sorting defect in bro1Δ cells. (A) *WT (SEY6210), bro1Δ (GOY65) or bro1Δ::TEF1p-Bro1CTF (CTY2) cells were transformed with the indicated GFP-tagged cargo plasmid to assess MVB sorting using live cell fluorescence microscopy. White dashed lines indicate cell boundaries. Scale bar = 5μm.*

Bro1 V domain stimulates Vps4 function in vitro

The possibility that V domain mediates Bro1 stimulation of Vps4 was assessed using ATPase assays with purified recombinant proteins as previously established [16,18]. Vps4 exhibits concentration dependent increases in specific activity due to Vps4 oligomer formation with maximal activity observed with 1.5μM Vps4[16,17]. Titration of Bro1V into ATPase assays with a submaximal concentration of Vps4 (0.5μM) showed a concentration dependent stimulation of activity with a maximum of 3-fold (Figure 3A). Stimulated activity of 0.5μM Vps4 did not surpass the inherent maximal Vps4 specific activity observed with 1.5μM Vps4, and Bro1V was unable to stimulate 1.5μM Vps4 specific activity (Figure 3A and data not shown). These observations suggest that Bro1V stimulates Vps4 oligomerization without further enhancing activity of the Vps4 oligomer. Furthermore, V domains from *S. castellii* Bro1 (residues 370-709) and *human* HD-PTP (residues 364-695) stimulated Vps4 ATPase activity in a similar dose-dependent manner (Figure 3B). Together, these results reveal that Bro1 V domain can enhance Vps4 ATPase activity directly, and suggest this stimulatory activity is conserved among homologs.

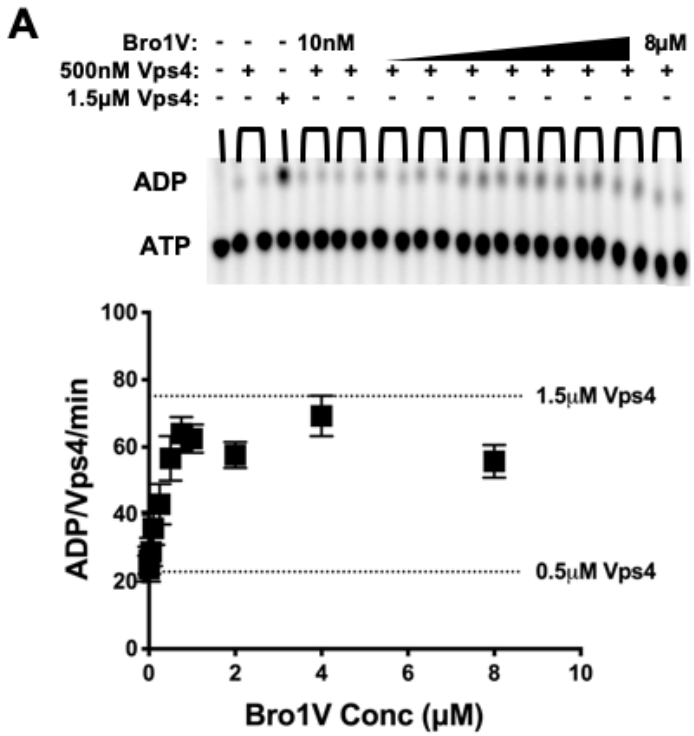

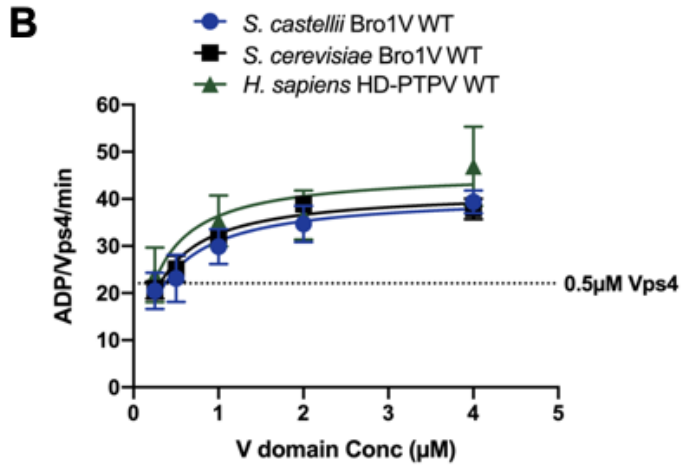

FIGURE 3. V domain stimulates Vps4 activity in vitro. (A) *Vps4 ATPase assays were conducted using the indicated conditions and resolved by thin layer chromatography for quantitation and calculation of hydrolysis rates. An image of the TLC plate raw data for a single time point (16min) is shown as an example of the data used for quantitation of Vps4-specific activities. ATPase activities across the titration of Bro1V (10nM – 8μM) in the presence of 0.5μM Vps4.* ***(B)*** *V domains of S. cerevisiae Bro1, S. castellii Bro1, and H. sapiens HD-PTP (0.5-4μM) were titrated against 0.5μM Vps4. Specific activity of Vps4 is expressed as ADP per Vps4 molecule per minute. Error bars indicate mean ± S.E.M. Dashed lines indicate Vps4-specific activity for 0.5μM or 1.5μM Vps4 alone, as indicated.*

169

170 *Rational generation and characterization of Bro1 V domain mutations defective for Vps4*
171 *stimulation*

172 Since we demonstrated that *S. cerevisiae* and *S. castellii* Bro1 V domains and *H. sapiens* HD-
173 PTP V domain stimulate Vps4 and interaction between *H. sapiens* ALIX and VPS4B has been
174 observed [58], we hypothesized that the mode of stimulation would be conserved. Conserved
175 surface residues shared amongst Bro1, HD-PTP and ALIX were mutated to map regions
176 involved in Vps4 stimulation (Figure 4A). Vps4 stimulation was measured using ATPase
177 reactions with the addition of WT or mutant forms of Bro1V (at a concentration found to support
178 maximal Vps4 activity in Figure 3A). Under these conditions four mutants — **Bro1V(M4)**:
179 V505A, H508A, I512A; **Bro1V(M8)**: E686A, L691D; **Bro1V(M20)**: T587D; and **Bro1V(M24)**:
180 K481D — were defective for stimulation of Vps4 ATPase activity, while other Bro1V mutants
181 displayed stimulation indistinguishable from WT V domain (Figure 4B). *In vitro* interaction
182 studies revealed that Bro1V(M4), Bro1V(M8), Bro1V(M20), and Bro1V(M24) retained their
183 abilities to bind Vps4 (Figure 4C, Figure 4 Supplement 1). The ability of these mutants to
184 associate with Vps4 led us to perform titration experiments to assess the impact on Vps4 ATPase
185 activity. These mutants were able to stimulate Vps4 ATPase activity at lower concentrations
186 ($\leq$1μM), whereas higher concentrations exhibited reduced stimulation or inhibition of Vps4
187 (Figure 4D). This profile contrasted with the behavior of WT V domain that continued to
188 stimulate Vps4 ATPase activity even at the highest concentrations tested. Together these
189 analyses suggest that V domain stimulation of Vps4 relies on determinants beyond mere binding
190 and indicate that these mutants specifically impact the stimulatory aspect of Vps4 regulation.
191

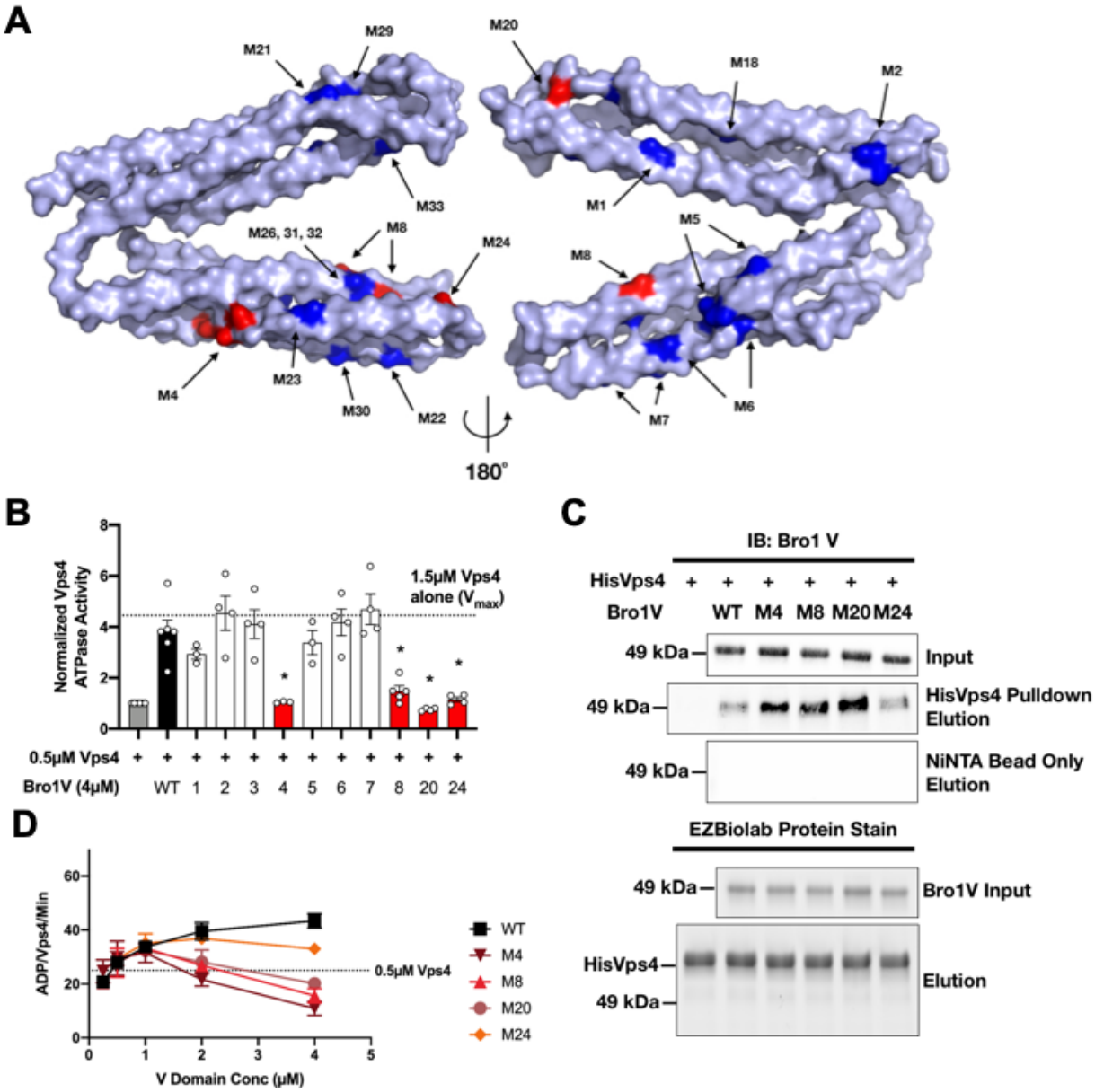

FIGURE 4. Mutations in Bro1 V domain disrupt Vps4 stimulation in vitro without disrupting binding. (A) *Model of the V domain based on the S. castelli Bro1 V domain crystal structure (Protein Data Bank ID: 4JIO, chain A) with amino acid substitution mutations impacting V domain stimulation of Vps4 indicated in red. Conserved residues that when mutated did not impact Vps4 stimulation in vitro or MVB sorting in vivo are indicated in blue. See Supplemental Table 4 for individual mutations.* ***(B)*** *Stimulation of Vps4 ATPase activity (0.5μM) by 4μM Bro1V(370-709) and Bro1V mutants represented as normalized Vps4 ATPase activity of at least two experiments done in duplicate. Error bars represent mean ± S.D. Statistical differences with the addition of Bro1V(M4), Bro1V(M8), Bro1V(M20), and Bro1V(M24) are indicated as red bars (*, $p < 0.05$).* ***(C)*** *Immobilized His_6-Vps4 or Ni-NTA beads alone was incubated with Bro1V,*

203 *Bro1V(M4), Bro1V(M8), Bro1V(M20), and Bro1V(M24). Bound material was visualized by both*
204 *EZBiolab Instant-Band Protein Stain and Western blotting with anti-Bro1 antiserum.* ***(D)***
205 *ATPase activities for the titration of Bro1V, Bro1V(M4), Bro1V(M8), Bro1V(M20), and*
206 *Bro1V(M24) (0.25-5μM) in the presence of 0.5μM Vps4. Vps4specific activity is expressed as*
207 *ADP per Vps4 molecule per minute. Error bars indicate mean ± S.E.M.*
208
209 The physiological significance of Vps4 stimulation by Bro1V was examined using cells
210 expressing the mutants forms of full-length *BRO1* to assess complementation of the *bro1*Δ MVB
211 sorting defect (Figure 5, Figure S3A, S3B). Three distinct model MVB cargoes were utilized for
212 this analysis: GFP-Cps1 for its strict dependence upon Ub modification for proper sorting, the
213 chimera Ub-GFP-Cps1 for its lack of dependence upon exogenous Ub modification, and Sna3-
214 GFP as a cargo that has been shown to access the MVB pathway both directly and via
215 association with other ubiquitinated cargoes [73,87-91]. Expression of Bro1(M4), Bro1(M8),
216 Bro1(M20), and Bro1(M24) in *bro1*Δ cells failed to complement the MVB sorting defects
217 observed with each cargo (Figure 5A) in spite of displaying protein levels similar to WT (Figure
218 5B, Figure S3C). The correlation between altered Vps4 stimulation and defects in MVB cargo
219 sorting observed with these mutants support the conclusion that V domain stimulation of Vps4 is
220 required for ESCRT-driven MVB cargo sorting *in vivo*.
221

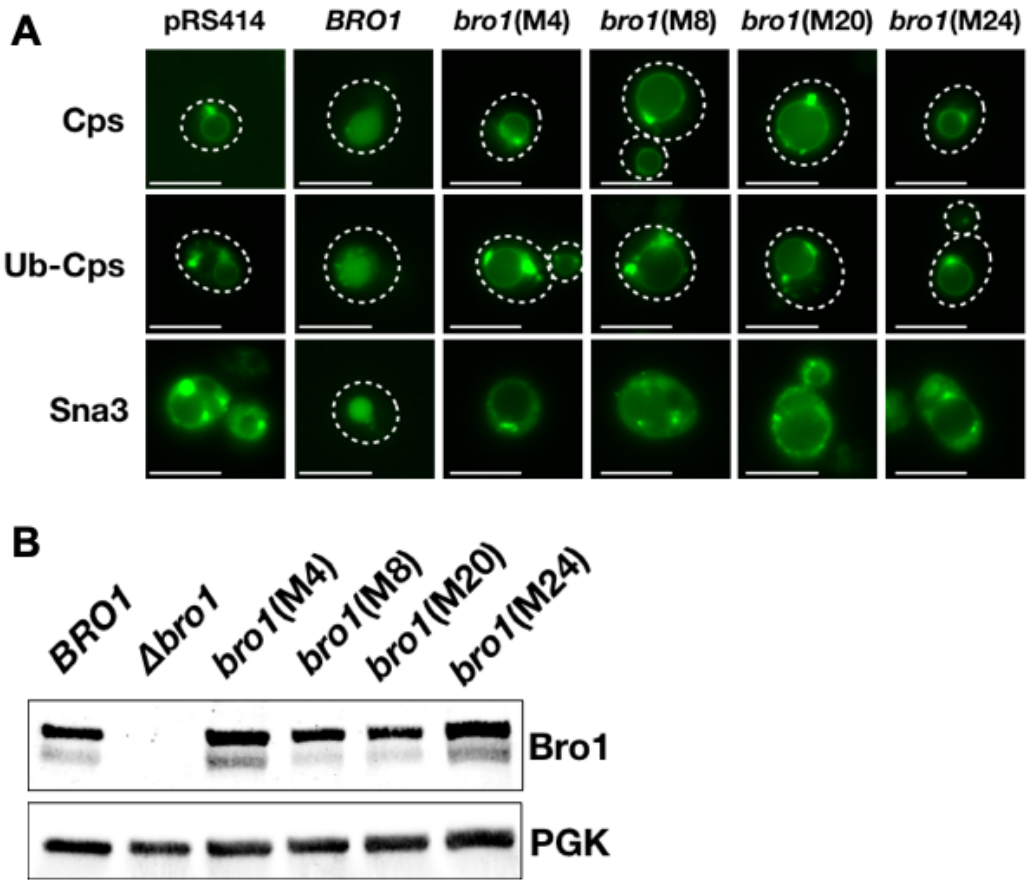

FIGURE 5. Bro1 V domain mutations disrupting Vps4 stimulation in vitro also disrupt MVB sorting in vivo. (A) *bro1Δ (GOY65) were transformed with empty plasmid (pRS414), or plasmid expressing BRO1, bro1(M4), bro1(M8), bro1(M20), or bro1(M24) together with model MVB cargo GFP-Cps1, Ub-GFP-Cps1 and Sna3-GFP to assess MVB sorting in these mutant contexts using live cell fluorescence microscopy.* ***(B)*** *Representative Western blots showing mutant protein expression levels, probing against Bro1 and PGK, using lysates of GOY65 transformed with empty plasmid (pRS414), or plasmid expressing BRO1, bro1(M4), bro1(M8), bro1(M20), or bro1(M24).*

Altered regulation of Vps4 activity by Bro1 perturbs ILV formation in vivo

To test whether disruption of V domain stimulation of Vps4 impacts ILV formation kinetics as assessed by the number and/or size of budding events, *bro1*Δ cells expressing Bro1(M8) were examined by dual axis electron tomography. Bro1(M8) cells displayed approximately twice as many ILV budding intermediates per MVB as compared to WT as well as reduction in the surface area of the budding profiles, while the ILV size was increased (Figure 6A, 6B, Figure 6 Supplement Movie 1). These observations suggest that disrupted Bro1 stimulation of Vps4 delays ILV budding and scission. Together, these results with Bro1(M8) (Figure 6) and

240 Bro1CTF (Figure 1) support a model in which the V domain of Bro1 stimulates Vps4 activity in
241 a manner that is critical for normal ILV formation kinetics.

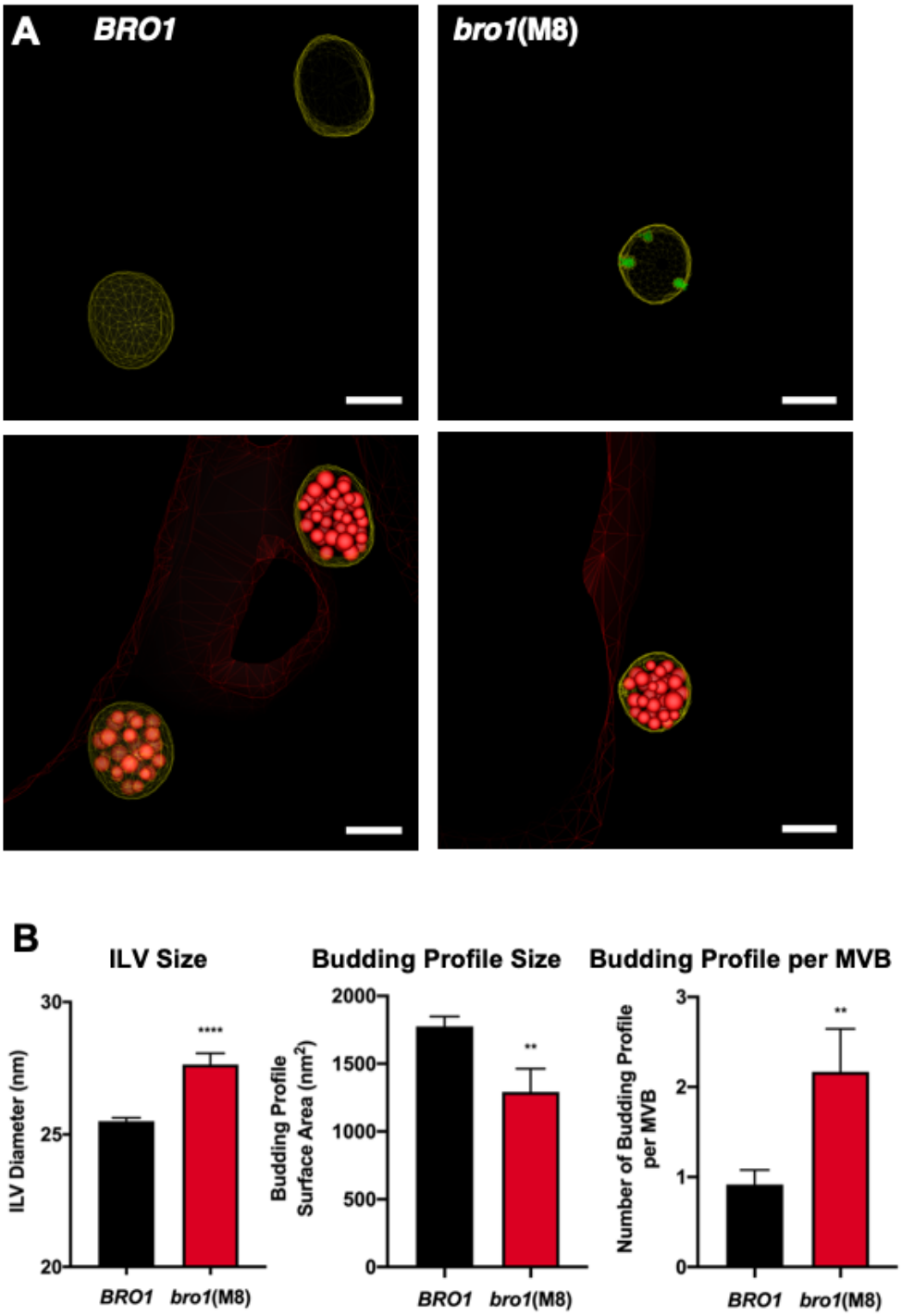

242
243 ***FIGURE 6. Cells expressing full length Bro1(M8) display increased number of ILV budding***
244 ***intermediates. (A)*** *Three-dimensional models reconstructed from 200-nm-thick section electron*
245 *tomograms of bro1Δ (GOY65) expressing either BRO1, or bro1(M8). The limiting membrane of*

246 *the MVB is labeled yellow, the ILVs are highlighted in red and the budding intermediates are*
247 *colored in green. The vacuolar membrane is labeled as red mesh. Scale bar = 100nm.* ***(B)***
248 *Quantification of electron tomograms of GOY65 expressing either BRO1, or bro1(M8).*
249 *Representative reconstructed image for cells expressing BRO1 and bro1(M8) are shown in (A).*
250 *A minimum of 6 MVBs and 94 ILVs from at least 4 cells were measured. Error bars indicate*
251 *mean ± S.E.M. Statistical significances are indicated (**, $p < 0.01$; ****, $p < 0.0001$).*
252
253 To determine if Bro1V stimulation of Vps4 influences ESCRT-III polymer dynamics, we tested
254 whether Bro1 mutants with altered Vps4 regulation also affected ESCRT-III disassembly.
255 Purified Bro1V domains (WT, M4, and M8) were titrated into *in vitro* Vps4-dependent ESCRT-
256 III disassembly reactions [16], and indistinguishable stimulation of Vps4 disassembly activity was
257 observed (Figure 7A). In addition, subcellular fractionation experiments showed WT levels of
258 the ESCRT-III subunit Snf7 on membranes for each of the Bro1 V mutations in the context of
259 full-length Bro1 (Figure 7B). These finding suggest that Bro1V-mediated Vps4 stimulation
260 impacts ESCRT-III function independent of ESCRT-III subunit disassembly/recycling.
261

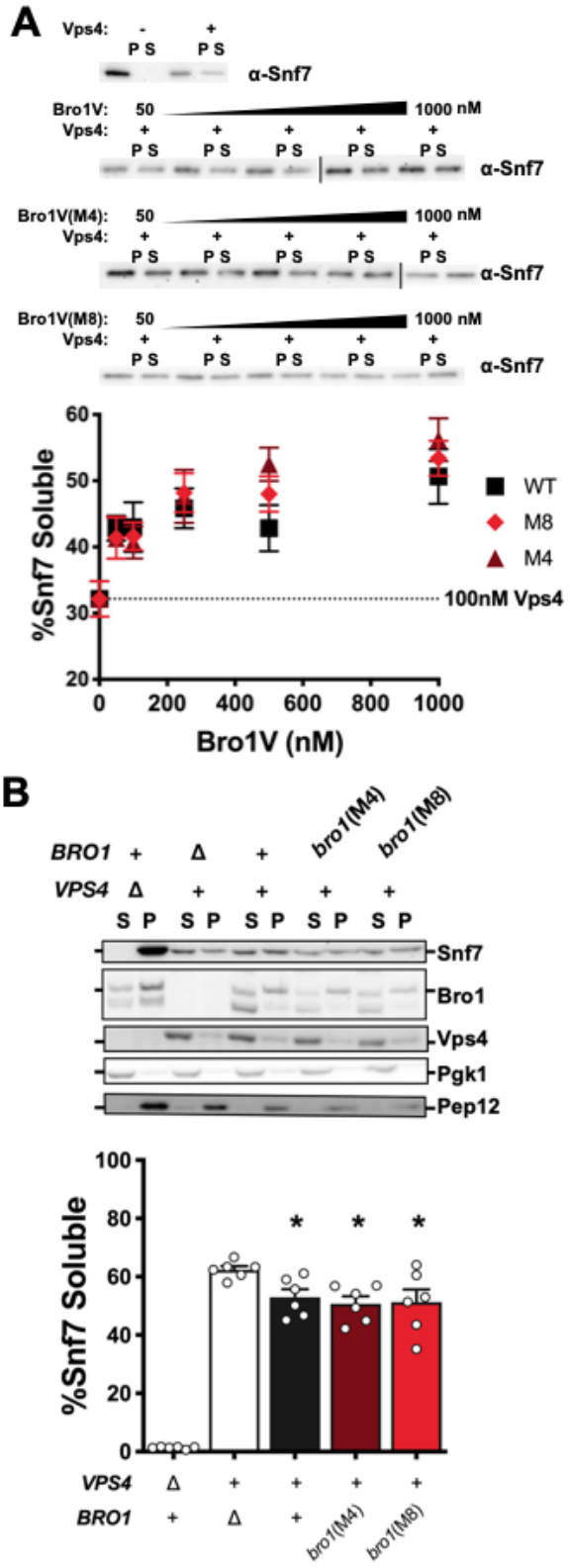

FIGURE 7. Bro1V M4 and M8 are not defective in their ability to stimulate Vps4-dependent ESCRT-III disassembly in vitro or in vivo. (A) *Bro1 V domains [Bro1V (black squares),*

265 *Bro1V(M4) (dark red triangles), Bro1V(M8) (light red diamonds)] (50-1000nM) were titrated*
266 *into Vps4-dependent ESCRT-III disassembly assay [16], containing 100nM Vps4. Representative*
267 *blots of Snf7 distribution between the pellet (P) and soluble fractions (S) are shown (upper*
268 *panels). Quantification of three experiments with reactions performed in duplicates is designated*
269 *as "% Snf7 soluble" (lower graph). Error bars indicate mean ± S.E.M.* ***(B)*** *Subcellular*
270 *fractionation was performed in bro1Δ (GOY65) cells transformed with an empty vector or*
271 *plasmids expressing BRO1, bro1(M4), or bro1(M8). vps4Δ (MBY3) cells were used as a control*
272 *highlighting the distribution upon complete loss of Vps4 function. Representative Western blots*
273 *showing fractionation of Snf7, Bro1, and Vps4 are shown. Pep12 and Pgk1 were used as*
274 *membrane and soluble markers respectively. Quantification represents six experiments, error*
275 *bars indicate mean ± S.E.M. Statistical significance is indicated relative to bro1Δ (*, $p < 0.05$).*
276
277 *Ubiquitin binding enhances Bro1 V domain stimulation of Vps4 activity and ILV formation in*
278 *vivo*
279 Bro1 binds Ub via a conserved motif at the amino-terminal portion of the V domain (Figure 8A)
280 [48]. While Bro1 has been implicated as a Ub-sorting receptor [48,86], how Ub-binding by Bro1
281 mediates cargo sorting and whether that binding helps integrate and regulate other aspects of ILV
282 formation is unclear. We hypothesized that Ub binding to the V domain impacts its stimulation
283 of Vps4. Addition of Ub to ATPase reactions increased Bro1V stimulation of Vps4 ATPase
284 activity *in vitro* (Figure 8B). In contrast, addition of Ub had no effect on Vps4 stimulation by a
285 Ub-binding defective V-domain mutant [Bro1V(I377R) "UBD-Mut"]. Similar results were
286 obtained using WT or Ub-binding deficient *S. castellii* V domain [Bro1V(I377R)[48]]. These
287 results indicate a conserved mode of Ub-dependent regulation of the V domain. We next tested
288 whether this Ub enhancement could occur in the Bro1V mutants that exhibit defective Vps4
289 stimulation. For this analysis, we used mutants Bro1V(M4) and Bro1V(M8) as these mutations
290 are spatially separated from the Ub-binding site (Figure 8C). Mutations that perturbed basal
291 stimulation of Vps4 also disrupted the ability of V domain to respond to the addition of Ub as the
292 slight increase in activity is not statistically significant (Figure 8D). Together these results 1)
293 demonstrate a conserved ability of Bro1 family V domains to stimulate Vps4 in a manner that
294 responds to Ub, and 2) suggest that Bro1 may serve as a Ub sensor to modulate ILV formation
295 via Vps4 *in vivo*.
296

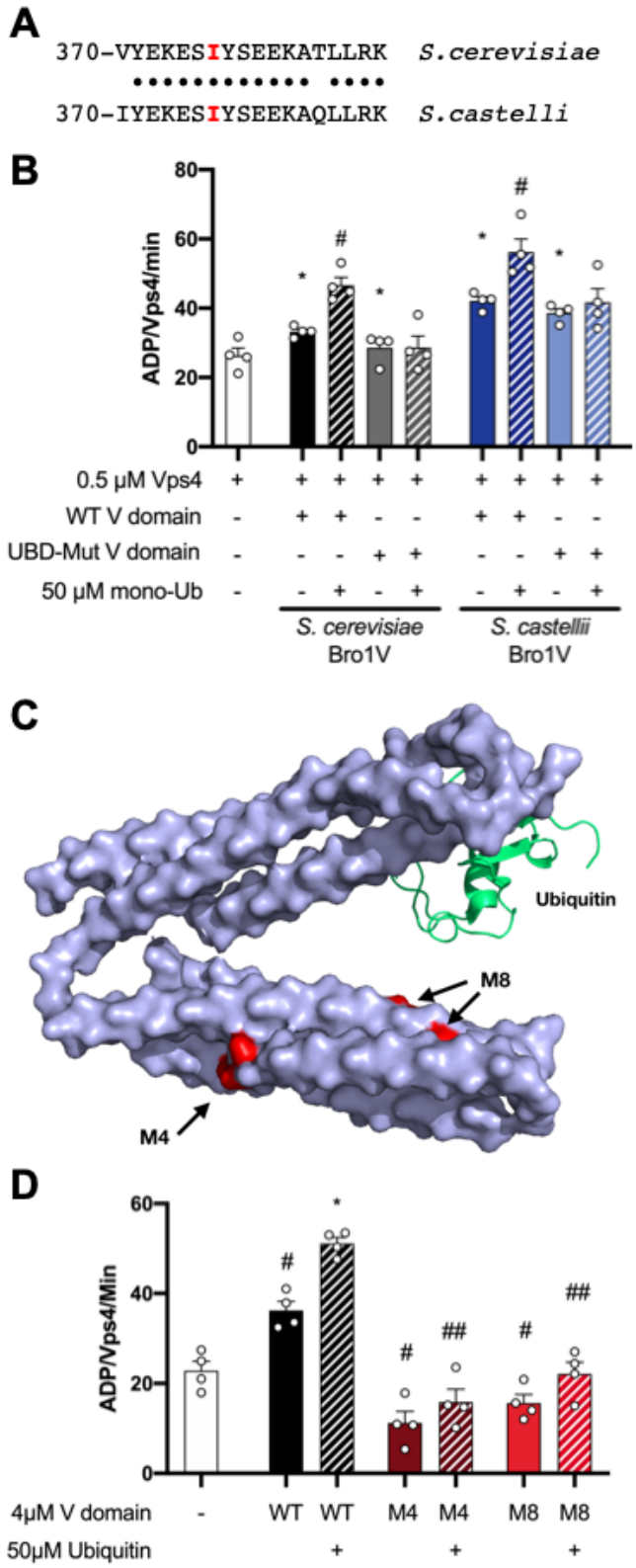

Figure 8. Ubiquitin is able to potentiate V domain-mediated stimulation of Vps4 ATPase activity. (A) *Sequence alignment of V domain amino acids 370-388 from S. castellii and S.*

300 *cerevisiae. Conserved amino acids are indicated by black circles, and the isoleucine critical for*
301 *ubiquitin binding is highlighted in red.* ***(B)*** *Analysis of stimulation of Vps4 ATPase activity*
302 *(0.5µM) by 1µM S. cerevisiae Bro1V, S. cerevisiae Bro1V(I377R, UBD-Mut), S. castellii*
303 *Bro1V(370-708) and S. castellii Bro1V(I377R, UBD-Mut) with or without 50µM of mono-Ub.*
304 *Vps4-specific activity is expressed as ADP per Vps4 molecule per minute. Error bars indicate*
305 *mean ± S.E.M. Statistical differences with the addition of WT V domain, V domain with Ub-*
306 *binding mutation, or Ub are indicated (* or #, $p < 0.05$).* ***(C)*** *Bro1 V domain mutations M4 and*
307 *M8 (red) that disrupt V domain stimulation of Vps4 ATPase activity are spatially separated from*
308 *its Ub-binding site using S. castellii Bro1V crystal structure (Protein Data Bank ID: 4JIO, chain*
309 *A).* ***(D)*** *Analysis of stimulation of Vps4 ATPase activity (0.5µM) by 4µM S. cerevisiae*
310 *Bro1V(370-709), Bro1(M4) and Bro1V(M8) with or without 50µM of mono-Ub. Vps4-specific*
311 *activity is expressed as ADP per Vps4 molecule per minute. Error bars indicate mean ± S.E.M.*
312 *Statistically significant differences compared to 0.5µM Vps4 alone are indicated (# or *, $p <$*
313 *0.05). (##) indicate both statistically different from Ub stimulated WT ($p < 0.0001$) and*
314 *difference between basal state stimulation and Ub addition is not significant.*
315
316 This model was tested in the context of Bro1CTF. Since cells expressing Bro1CTF as their sole
317 form of Bro1 generate ILVs but fail to sort MVB protein cargoes, we utilized the fluorescent
318 lipid analog NBD-PC as a rapid, quantifiable indicator of ILV formation (Figure 9A, Figure 9
319 Supplement 1). NBD-PC accumulates in the vacuole lumen of WT cells, while NBD-PC sorting
320 is disrupted in ESCRT mutants ([92-94], and Figure 9A, 9B). Expression level of Bro1 fragments
321 were comparable by Western blotting (Figure 9C), and over-expression of full-length Bro1 did
322 not disrupt NBD-PC sorting (Figure 9B). Cells expressing the Bro1CTF resulted in a higher
323 number of cells with lumenal NBD-PC labeling compared to *bro1*Δ cells (40% versus 7%), and
324 this sorting was dependent upon both Vps4 (*TEF1p*-Bro1CTF *vps4*Δ: 0%) and the Bro1 PRR
325 (*TEF1p*-Bro1V: 7%). While Bro1CTFΔUBD also enhanced the number of cells with lumenal
326 NBD-PC labeling compared to *bro1*Δ cells (20% versus 7%), this enhancement was significantly
327 reduced compared to Bro1CTF (20% versus 40%). These results both reveal the dependence of
328 Bro1CTF ILV formation upon ESCRT function and support the model that Bro1 Ub binding
329 promotes ILV formation via Vps4.
330

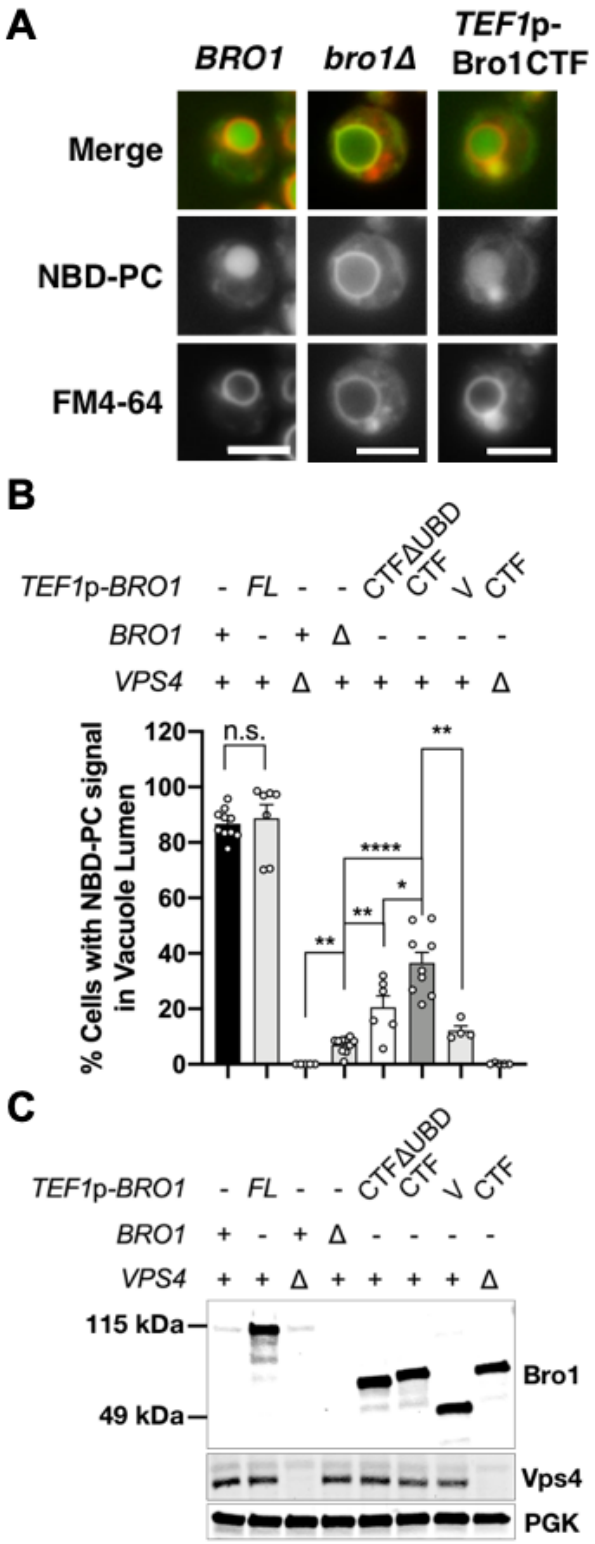

331

332 ***FIGURE 9. Bro1CTF supports sorting of NBD-PC into the vacuolar lumen, is dependent on***
333 ***Vps4, and is enhanced by the ability to bind Ub. (A)*** *Sample micrographs of WT (SEY6210),*

334 *bro1Δ (GOY65), and bro1Δ::TEF1p-Bro1CTF (CTY2) cells co-stained with NBD-PC and FM4-*
335 *64 revealing endpoints of the observed phenotypes. Scale = 5µm.* ***(B)*** *NBD-PC and FM4-64*
336 *stained WT, vps4Δ (MBY3), bro1Δ, bro1Δ::TEF1p-Bro1 (CTY1), bro1Δ::TEF1p-Bro1CTF*
337 *(CTY2), bro1Δ::TEF1p-Bro1CTFΔUBD (CTY3), bro1Δ::TEF1p-Bro1V (CTY4), and*
338 *vps4Δ::TRP1 bro1Δ::TEF1p-Bro1CTF (CTY5) cells were analyzed by live cell fluorescence*
339 *microscopy and quantified for the frequency of cells able to support NBD-PC trafficking to the*
340 *vacuolar lumen. Error bars indicate mean ± S.E.M. Statistical significances are indicated (n.s.,*
341 *not significant; *, p = 0.0167; **, p = 0.0012; ****, p < 0.0001).* ***(C)*** *SEY6210, MBY3, GOY65,*
342 *CTY1, CTY2, CTY3, CTY4, and CTY5 were analyzed by Western blotting using antibodies*
343 *against Bro1, Vps4 and PGK (as a loading control) expression levels.*
344
345 **Discussion:**
346 Here we describe an additional Bro1 activity relevant to ESCRT-dependent membrane
347 remodeling whereby the V domain directly stimulates Vps4 ATPase activity. Our studies reveal
348 2 key findings with respect to Bro1 function in ESCRT-dependent ILV formation that warrant
349 additional consideration: 1) V domain stimulation of Vps4 contributes to ILV formation and
350 MVB sorting *in vivo*, and 2) Ub enhances V domain stimulation of Vps4 *in vitro* and appears to
351 contribute to ILV formation *in vivo*, suggesting a novel role for Ub in ESCRT-mediated MVB
352 biogenesis beyond cargo recognition. Additionally, this work indicates aberrant activation of
353 ESCRT membrane remodeling activity via Bro1 can lead to spurious vesicle formation. The
354 ability of the Bro1CTF to dissociate cargo sorting from ILV formation suggests that Bro1 plays a
355 role in "licensing" ESCRT-III and Vps4 to drive membrane remodeling.
356
357 A number of factors have been documented to impact Vps4 ATPase activity: Vps4 concentration
358 itself, its co-factor Vta1, and interactions with ESCRT-III subunits [17,41,42,51]. Our previous
359 analyses have revealed that perturbations leading to reductions in the stimulated maximal activity
360 of Vps4 correlate with defects in Vps4-dependent ESCRT-III disassembly *in vivo* and *in vitro*
361 and are consistent with a model wherein the relevant activity of Vps4 is to disassemble the
362 ESCRT-III polymer coincident with or subsequent to ILV formation. In contrast, the mutant
363 forms of Bro1 characterized in the present work display defective Vps4 ATPase stimulation *in*
364 *vitro* and MVB sorting phenotypes *in vivo*, however the nature of that defect does not appear to
365 be at the level of ESCRT-III disassembly. Previous work has revealed that Vta1 and ESCRT-III
366 subunits can impact both assembly (K_m) and the maximal activity (V_{max}) of the Vps4 oligomer
367 [42,51]. Our biochemical analysis suggests that V domain facilitates assembly of the Vps4 oligomer
368 (Figure 3). Based on these findings, we propose that factors capable of contributing to increased
369 maximal Vps4 activity contribute to ESCRT-III disassembly (e.g. Vta1, ESCRT-III subunits)

370 while factors that contribute solely to driving oligomerization (e.g. Bro1) contribute to earlier
371 events during ILV biogenesis.
372
373 The hypothesis that Bro1-mediated Vps4 oligomerization contributes to ILV expansion and
374 scission is supported by analysis of MVB morphology. Bro1(M8) is defective for Vps4
375 stimulation and displayed both increased numbers of endosomal budding profiles and decreased
376 surface area of the endosomal budding profiles. Overexpression of BOD or full-length Bro1 in
377 WT yeast also generated increased endosomal budding profile numbers, however the surface
378 area of the budding profiles was not impacted [26]. These effects with overexpression of BOD or
379 full-length Bro1 correlated with reduced Vps4-mediated disassembly of ESCRT-III *in vitro* and
380 *in vivo*, suggesting that decreased kinetics of ESCRT-III dynamics results in increased numbers
381 of endosomal budding profiles. The correlation of reduced Vps4 ATPase stimulation in the
382 context of Bro1V(M8) with increased, smaller budding profiles in *bro1(M8)* suggests that
383 stimulation of Vps4 by Bro1 contributes to an early stage of ILV biogenesis such as the
384 expansion of the nascent bud. Vps4 recruitment to the site of MVB sorting occurs in two phases:
385 an early, minimal recruitment of Vps4 oligomers associated with stable ESCRT-III membrane
386 association followed by a later recruitment of additional Vps4 oligomers implicated in ILV
387 formation and eventual ESCRT-III disassembly [19]. Our biochemical analysis indicating that V
388 domain facilitates Vps4 oligomerization (but not maximal activity) is consistent with Bro1
389 contributing to either early or late Vps4 recruitment. While ESCRT-III itself has been suggested
390 to facilitate Vps4 recruitment and stimulation [27,42], this study reveals Bro1 V domain
391 contributions to this process are required for normal MVB protein cargo sorting. One possibility
392 would be that an incomplete cohort of ESCRT-III subunits during the expansion phase maintains
393 dependence upon V domain contribution to Vps4 activity, whereas the accumulation of
394 additional ESCRT-III subunits completes the expansion phase and permits progression to
395 disassembly. Another possibility is that the disassembly phase exhibits reduced accumulation of
396 Bro1, as M4 and M8 mutants were not defective for ESCRT-III disassembly and low
397 concentrations of Bro1V(M4) and Bro1V(M8) exhibit similar stimulation of Vps4 ATPase
398 activity similar to WT. Consistent with this model, reduction of Bro1 during the disassembly
399 phase would relieve inhibition conferred by elevated Bro1 or BOD [26]. Further studies will be
400 needed to understand the dynamics and unique contributions of Bro1 in regulating Vps4 function
401 during MVB sorting.
402
403 Our results implicate Ub-binding to the V domain as a point of modulation during ILV formation
404 beyond cargo selection. Previous studies demonstrated a role for Ub in MVB sorting at the level
405 of cargo recognition [87,94,95] as well as the dependence of ILV formation on the presence of Ub-
406 cargo [95,96]. However, upstream effects on cargo recognition and early ESCRT membrane

407 recruitment precluded examination of the role of Ub in ILV formation itself. Our studies with
408 Bro1CTF suggest that Ub-binding also contributes to ILV formation as Bro1CTF exhibited
409 greater NBD-PC sorting into the vacuole lumen than Bro1CTFΔUBD. The abilities of the V
410 domain to stimulate Vps4 ATPase activity and bind to Ub afforded an opportunity to examine
411 whether Ub impacts this regulation. Our results suggest Ub regulation of V domain stimulation
412 of Vps4 is a conserved feature within the Bro1 family. ALIX also binds VPS4B and Ub,
413 however the association between ALIX and Ub appears distinct from the Bro1 V interaction with
414 Ub [53,55]. Thus, further studies are required to determine if Ub regulation of V domain stimulation
415 extends to ALIX as well. The source of Ub *in vivo* remains to be determined, but could result
416 from a variety of sources including Ub-cargo, ubiquitination of Bro1 itself [97], or free Ub
417 resulting from the recruitment of DUbs via Bro1 family members [45]. Our results suggest a role
418 for Bro1 Ub-binding in modulating ILV formation via Vps4 in addition to the previously
419 appreciated role in facilitating cargo recognition.
420
421 The general link between ILV formation and the delivery of protein cargo into the forming ILV
422 is poorly defined, but our studies suggest Bro1 helps couple these functions. While ESCRT-III
423 and Vps4 serve as the core ILV formation machinery, targeting chimeric deubiquitylating
424 constructs to the site of MVB sorting disrupted protein cargo sorting as well as ILV formation,
425 indicating that Ub-cargo itself contributes to ILV formation [96]. When expressed as the sole
426 source of Bro1, Bro1CTF creates a contrasting phenomenon wherein ILV formation is restored
427 without concomitant protein cargo sorting. This phenomenon has also been observed with
428 disruption of Ub-binding activities of ESCRT-I and -II in conjunction with disruption of
429 ESCRT-0 and -I interaction [94]. While the relationship between these two contexts is presently
430 unclear, these phenomena indicate that ILV formation can occur in the absence of protein cargo
431 sorting. Bro1 mutants defective for Vps4 stimulation also perturb protein cargo sorting while
432 ILV formation is retained, although with altered kinetics. Disrupted MVB protein cargo sorting
433 with Bro1CTF (with increased ILV formation kinetics), as well as with Bro1 mutants defective
434 for Vps4 stimulation (with delayed ILV formation kinetics), suggest a model in which Bro1
435 facilitates MVB cargo sorting through properly regulating Vps4 and ESCRT-III dynamics
436 driving ILV formation (Figure 10). We suggest that Bro1 serves to "license" ILV formation,
437 typically coordinated with cargo entry to enable efficient MVB sorting. Overexpression of ALIX
438 enhances the release of HIV particles as well as small extracellular vesicles [54,98], consistent with
439 ALIX being rate-limiting in these processes and potentially serving as a licensing factor for these
440 ESCRT-mediated events in human cells as well. Thus, we suggest that Bro1 family members —
441 with their various modes of interaction with Ub-cargo, deubiquitinating enzymes, and other
442 ESCRT subunits — serve to regulate Vps4 recruitment and ESCRT-III dynamics to facilitate
443 cargo transfer and ILV formation enabling MVB cargo sorting.

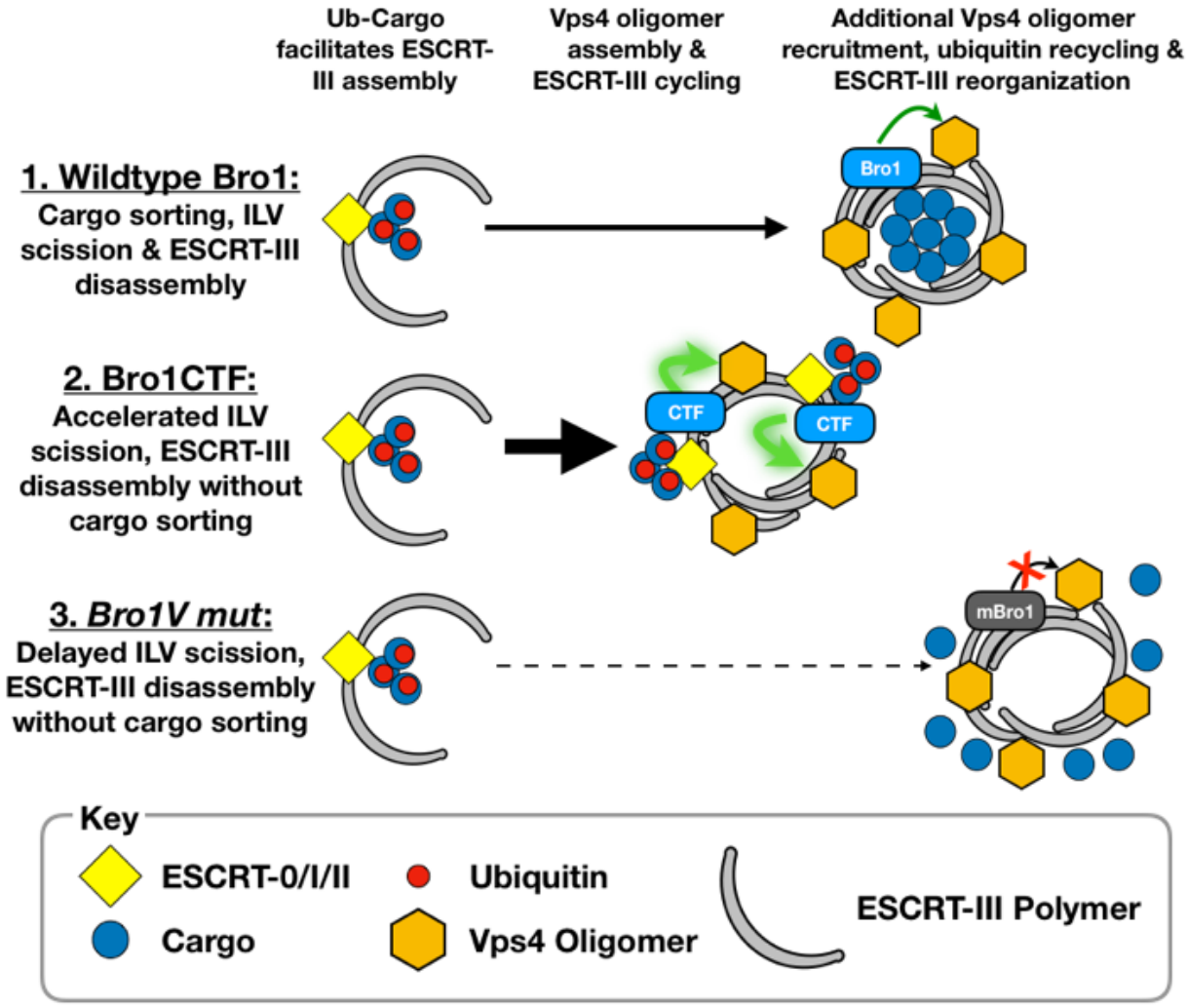

FIGURE 10. Model for Bro1 regulation of Vps4 and impact upon ESCRT-III dynamics. (1) *We propose that subsequent to cargo clustering via early ESCRTs (-0, -I, -II) and initiation of ESCRT-III assembly, Bro1 stimulates Vps4 to coordinate cargo sorting into the budding ILV such that the resulting ILV contains cargo.* ***(2)*** *When Bro1CTF is the sole form of Bro1, the increase in V domain activity stimulating Vps4 uncouples ILV expansion and MVB cargo sorting.* ***(3)*** *When Bro1 V domain mutants (mBro1) that are defective for stimulating Vps4 are the sole form of Bro1, the lack of Vps4 stimulation delayed ESCRT-III disassembly, resulting in delayed ILV formation and disrupted cargo sorting for the concentrated cargo microdomain became diffuse.*

455 **List of Supplementary Figures:**

456 Figure 1:

457 Figure 1 Supplement 1. Electron tomography of WT cells expressing Bro1CTFΔUBD.

458 Figure 1 Supplement Movie 1. Tomogram of MVB in a WT cell.

459 Figure 1 Supplement Movie 2. Tomogram of MVB in a WT cell expressing Bro1CTFΔUBD.

460 Figure 1 Supplement Movie 3. Tomogram of MVB in a *bro1*Δ cell.

461 Figure 1 Supplement Movie 4. Tomogram of MVB in a *bro1*Δ::*TEF1p*-Bro1CTF cell.

462

463 Figure 4:

464 Figure 4 Supplement 1. Bro1 V domain mutants still bind Vps4.

465

466 Figure 5:

467 Figure 5 Supplement 1. Evaluating the expression and the impact on cargo sorting of Bro1 V

468 domain mutants.

469

470 Figure 6:

471 Figure 6 Supplement Movie 1. Tomogram of MVB in a *bro1*Δ cell expressing Bro1(M8).

472

473 Figure 9:

474 Figure 9 Supplement 1. Representative images of cells stained with NBD-PC and FM4-64.

475

476 **Methods:**

477 *Plasmids and Strains*

478 For a complete listing of plasmids utilized in this study see Supplemental Table 1. The sequence
479 encoding the V-domain of Bro1 (Bro1V, aa 370-709) was amplified from pGO216 [26] and cloned
480 into the *Bam*H1 and *Sal*I sites of pGST-parallel1 [70] to generate pSD1. *BRO1* was amplified from
481 pGO187 [71] and cloned into the *Spe*I and *Sal*I site of pRS414 [72] to generate pSD12. Mutagenesis
482 of Bro1V or *BRO1* encoding constructs (pSD2-9, pSD13-14, pCT2, pCT4-8, pCT10, pCT13-16,
483 pCT18, pCT20-24, pCT26, and pCT29-33 was performed using the GeneTailor Site-Direct
484 Mutagenesis System (Life Technologies, Carlsbad, CA). The veracity of plasmids was confirmed
485 by sequencing. The sequence encoding $Bro1^{BODV}$ (aa 1-709) was amplified from pGO216 and
486 cloned into *Bam*H1 and *Sal*I sites of pET28b (Novagen, Germany) and pGST-parallel1 for use
487 generating and purifying the anti-Bro1 sera, respectively (see *Bro1 antibody generation*).

488 Two silent mutations (D133D, D153D) were introduced into the *HIS3* cassette of pRS413
489 to remove undesired *Bgl*II sites by site-directed mutagenesis; the resulting plasmid was named
490 pCT34. The sequence encoding *HIS3* cassette was amplified from pCT34 by PCR to introduce
491 *Bam*HI and *Pac*I sites, and cloned into *Bgl*II and *Pac*I sites of pFA6a-HisMX6; the resulting
492 plasmid is named pCT35. The sequence encoding Bro1V(370-709) was amplified from
493 SEY6210 genomic DNA, and cloned into *Nco*I and *EcoR*I sites of pCT35; the resulting plasmid
494 is named pCT36. Subsequently, 500bp of *BRO1* 3'UTR was amplified from SEY6210 genomic
495 DNA and cloned into *EcoR*I and *Sac*I sites of pCT35; the resulting plasmid is named pCT37.
496 DPAP-B-GFP was cloned from pGO89 [73] into *Not*I and *Sal*I sites of pRS425; the resulting
497 plasmid is DPAP-B-GFP. For a list of primers used to generate pCT34, pCT35, pCT36 and
498 pCT37, please see Supplemental Table 2.
499 For a complete listing of strains used in this study see Supplemental Table 3. CTY1,
500 CTY2, and CTY3 were generated by transforming PCR product from pCT34 into SEY6210.1
501 while CTY4 was generated by transforming PCR product from pCT36; for a list of primers used,
502 please see Supplemental Table 2. Transformants were plated on Histidine drop-out synthetic
503 plates, and screened by Western blotting. The altered *bro1* allele was amplified and sequenced.
504 CTY5 and JPY403 was generated using standard yeast genetics.
505
506 *Protein expression and purification*
507 Protein expression was performed in the BL21-DE3 bacterial strain using 0.5 mM isopropyl β-d-
508 1-thiogalactopyranoside (IPTG) at 16°C for 18-22hrs. GST-Bro1V fusion protein and mutants
509 thereof were purified using the Glutathione Sepharose 4B (GE Healthcare, United Kingdom),
510 treated with AcTEV protease (Thermo Fisher Scientific, Waltham, MA) overnight at room
511 temperature to remove the GST tag, incubated with ATP to dissociate chaperones, and subjected
512 to size-exclusion chromatography (Superdex200 HiLoad 16/60) in 25mM HEPES and 150mM
513 KCl. Purified proteins were tested for purity using SDS-Page and Coomassie staining and were
514 analyzed to exclude contaminating ATPase activity (data not shown). All Bro1V mutants
515 examined in this study exhibited equivalent expression levels in bacteria (data not shown) and
516 mutants expressed in yeast were at levels similar to WT (Figure 6b). GST-Vps4 was expressed
517 and purified as previously described for use in the ATPase assays [18]. His_6-Vps4 was purified as
518 previously described [43], except the His_6 fusion tag was not cleaved in order to use His_6-Vps4 in
519 the *In vitro* Binding Assays. His-Bro1^{BODV} purified from BL21-DE3 using Ni^{2+}-affinity
520 chromatography (5ml HiTrap Chelating FF column; GE Healthcare, United Kingdom). GST-
521 Bro1V(370-709) was purified using the Glutathione Sepharose 4B (GE Healthcare, United
522 Kingdom) and eluted with reduced glutathione (Thermo Fisher Scientific, Waltham, MA). V
523 domains of *S. castellii* Bro1 and human HD-PTP were produced in *E. coli* BL21 (DE3) were
524 purified over TALON-Co^{2+} and size exclusion chromatography and cleaved from their 6xHis tag

525 with AcTEV protease [48]. Mono-Ub was expressed in *E. coli* BL21 (DE3) from pPL5293. The
526 protein was purified from bacterial cell lysate by precipitation with 5% Perchloric acid and CMC
527 cation exchange chromatography in 0.05M ammonium acetate buffer pH 4.5 followed by elution
528 with 0.1M ammonium acetate buffer pH 5.5 [74].
529
530 *Antibody generation*
531 Anti-Snf7 antiserum was generated against GST-Snf7. Antiserum was generated in a New
532 Zealand rabbit (Covance, Princeton, NJ). Bleeds were evaluated for detection of Snf7 (SEY6210
533 and *snf7*Δ*)*. The Snf7 antibody was used at 1:5,000. Anti-Bro1 antiserum was generated against
534 His_6-Bro1^{BODV}. Antiserum was generated in a New Zealand rabbit (Covance, Princeton, NJ).
535 Antibodies were purified using GST-Bro1^{BODV} immobilized on an AminoLink column (Thermo
536 Fisher Scientific, Waltham, MA) and verified for sensitivity and specificity using yeast extracts
537 (SEY6210 and *bro1*Δ) and recombinant Bro1V. The purified Bro1 antisera was used at 1:1,000.
538
539 *In vitro* binding assays
540 Ni-NTA Agarose beads (Qiagen, Germany) +/-His_6-Vps4 (10µg) was incubated for 1 hr at 4°C
541 in NiA buffer (25mM NaH_2PO_4, 300mM NaCl, pH 7.5), washed with NiA buffer, and
542 equilibrated with ATPase buffer (see *ATPase assay*). Binding reactions were performed in
543 Handee Spin Columns (Pierce) with 6µg Bro1V or mutants in ATPase buffer + 0.02% Tween20
544 incubated for 1 hour at 30°C. Reactions were washed four times with NiA buffer with 10mM
545 imidazole (Sigma Aldrich, St. Louis, MO), and the bound material was eluted with NiA buffer
546 with 200mM imidazole. Instant-Bands Protein Stain (EZBiolab, Parsippany, NJ) were used to
547 visualize input and eluted material on a Typhoon FLA 7000 (GE Healthcare, United Kingdom).
548 Samples were resolved via SDS-PAGE, and detected using Western blotting against Bro1.
549 Bro1V input and His_6-Vps4 were detected via SDS-PAGE followed by Coomassie staining (data
550 not shown). Three or more independent experiments were performed with each experiment
551 performed in replicates within the experiment and representatives are shown. Data was graphed
552 and statistical significance was assessed by T tests using Prism 5 (GraphPad, San Diego, CA).
553
554 *ATPase assays*
555 Measurement of Vps4 ATPase activity was performed in ATPase buffer (20 mM HEPES, 100
556 mM KOAc, 5mM MgOAc, pH 7.5) as previously described [16,17,42,43,47,51] All reactions were
557 incubated at 30°C for 30 minutes prior to initiation by ATP addition (4mM final concentration).
558 Images were captured using a Typhoon FLA 7000 (GE Healthcare, United Kingdom). Data
559 represent ATPase activities from a minimum of three independent experiments with each
560 experiment performed in replicates within the experiment. Data was graphed and statistical
561 significance was assessed by T tests using Prism 5 (GraphPad, San Diego, CA). An example of

562 this analysis, including phosphorimager scans of the thin-layer chromatography (TLC) plates,
563 has been presented in Figure 3 [47]. The Vps4 concentration used was 0.5μM because this
564 concentration of Vps4 exhibits sub-maximal specific activity. ATPase assays in the presence of
565 Ub were performed with the minimal concentration (50μM) yielding maximal enhancement.
566
567 *ESCRT-III disassembly assays*
568 ESCRT-III disassembly assays were performed as previously described [16,51]. Briefly,
569 spheroplasted yeast (*vps4*Δ *pep4*Δ *bro1*Δ) were lysed with a Dounce homogenizer in 20mM
570 HEPES, 200mM Sorbitol, 50mM KOAc, 2mM EDTA, pH 6.8, and subjected to a 5 minute,
571 500xg clearing spin. The resulting supernatant was then spun 10 minutes at 13,000xg. Using
572 Disassembly Assay buffer (20mM HEPES, 100mM KOAc, 5mM MgOAc, 200mM Sorbitol, pH
573 7.4 with protease inhibitors), the pelleted membranes were washed and then resuspended at 50
574 OD_{600} equivalents/ml. Reactions were setup with 0.5 OD_{600} equivalents/ml, an ATP regeneration
575 system (1mM ATP) and various amounts of Vps4 and Bro1V. Vps4 and Bro1V were allowed to
576 preincubate prior to reaction initiation. The reactions were initiated by brief centrifugation
577 followed by incubation at 30°C for 10 min. Reactions were terminated by centrifugation at
578 13,000xg for 10 min. Western blotting analysis was used to assess the levels of Snf7 in the pellet
579 and soluble fractions. Snf7 was detected using anti-Snf7 polyclonal antibody (1:5000), HRP-
580 conjugated Goat anti- Rabbit IgG (Life Technologies, Carlsbad, CA, 1:30,000) and the UVP
581 Autochemi System (Upland, CA) and quantified using ImageQuant software (GE Healthcare,
582 United Kingdom). Linearity of the signal was confirmed via image histograms. Disassembly
583 assay data represent three independent experiments with each experiment performed in replicates
584 within the experiment. Data was graphed and statistical significance was assessed by T tests
585 using Prism 5 (GraphPad, San Diego, CA). Data are graphed as the mean with the standard error
586 of the mean, and representative Western blots are shown.
587
588 *Fluorescence microscopy*
589 For live-cell imaging of cells expressing GFP-tagged cargoes yeasty were grown in minimal
590 media at 26°C to mid-log phase ($0.5OD_{600}$) for live-cell fluorescence microscopy. Mup1-GFP
591 induction was accomplished by adding 50μM copper sulfate/chloride, as previously described [75].
592 Images were captured using an Olympus IX70 fluorescence microscope (Center Valley, PA)
593 with an FITC filter and digital camera (Coolsnap HQ; Photometrics, Tucson, AZ). Images were
594 deconvolved using Delta Vision software (Applied Precision, Issaquah, WA) and visualized
595 using FiJi (version: 2.0.0-rc-43/1.50i, National Institutes of Health, Bethesda, MD) [76]. Images
596 were captured on three different days using two different sets of transformations. Verification of
597 Bro1 and mutant Bro1 expression in these cells was confirmed by Western blotting.
598

599 Co-labelling with FM4-64 and C6-NBD-PC (Avanti Polar Lipids, Alabaster, AL) was performed
600 by incubating log-phase cells in YPD or Synthetic Media containing 1µM C6-NBD-PC and
601 250nM FM4-64 for 30 minutes at 30°C. Cells were then washed and chased for 1 hr at 30C.
602 Images were captured using an Olympus IX70 fluorescence microscope (Center Valley, PA)
603 fitted with FITC and rhodamine filters and digital camera (Coolsnap HQ; Photometrics, Tucson,
604 AZ). Cells with vacuolar lumenal NBD-PC signal were scored manually. Data represent
605 quantification from a minimum of four independent labeling experiments with each experiment
606 quantified at least 100 cells. Statistical significance was assessed by T tests using Prism 5
607 (GraphPad, San Diego, CA).
608
609 *Subcellular fractionations*
610 Subcellular fractionations were performed by osmotic lysis as previously described [77], except the
611 cell extracts were centrifuged at 13,000xg for 10 min at 4°C to separate the soluble and pellet
612 fractions [51]. Samples (0.1 or 0.2 OD_{600} equivalents) were resolved via SDS-PAGE and Western
613 blotted for Snf7 (this study, 1:5,000), Vps4 ([18], 1:1000), Bro1 (this study, 1:1,000). Pgk1 (Life
614 Technologies, Carlsbad, CA, 1:10,000), and Pep12 (Life Technologies, Carlsbad, CA, 1:1,000).
615 Western blots were developed using HRP-conjugated Goat anti-Rabbit (Life Technologies,
616 Carlsbad, CA, 1:30,000) or Goat anti-Mouse (Life Technologies, Carlsbad, CA, 1:1,000),
617 SuperSignal West Pico and SuperSignal West Femto substrates (Thermo Fisher Scientific,
618 Waltham, MA), and the UVP Autochemi System (Upland, CA). Signal was quantified using
619 ImageQuant software (GE Healthcare, United Kingdom). Signal linearity was confirmed via
620 image histograms. Data represent three or more independent experiments (representative
621 Western blots are shown) and are graphed as mean with standard error of the mean. Statistical
622 significance was assessed by T tests using Prism 5 (GraphPad, San Diego, CA).
623
624 *Statistical Analysis*
625 Statistical significance was assessed by parametric unpaired two-tailed Student's T test.
626
627 *Molecular modeling*
628 Molecular graphics and analyses of the *S. castelli* Bro1 V domain (Protein Data Bank ID: 4JIO,
629 chain A) were performed with the UCSF Chimera package and PyMOL[78,79]. Chimera was
630 developed by the Resource for Biocomputing, Visualization, and Informatics at the University of
631 California, San Francisco (supported by NIGMS P41-GM103311).
632
633 *Dual axis electron tomography*
634 Yeast cells were high-pressure frozen (HPF) and freeze-substituted (FS) as previously described
635 [80,81]. Liquid cultures were harvested during log phase and filtered with 4.5-micron Millipore

636 paper, collected into 0.5 mm aluminum hats, high pressure frozen with a Wohlwend HPF
637 (Wohlwend, Switzerland), and transferred to FS media kept at liquid nitrogen temperature until
638 cryo-fixation. Cells were then freeze-substituted in an AFS (Automated Freeze-Substitution
639 machine, Leica Vienna, Austria) at -90°C in cryo media made from 0.1% uranyl acetate 0.25%
640 glutaraldehyde in anhydrous acetone, washed in pure acetone, and embedded at -60°C in
641 Lowicryl HM20 (Polysciences, Warrington, PA). Samples were polymerized at -60°C with and
642 warmed slowly over four days. Plastic blocks were trimmed and sections were cut in 80 nm thin
643 sections and 250 nm thick sections with a Leica UC6 ultra-microtome and placed on Rhodium-
644 plated copper slot grids (Electron Microscopy Sciences, Hatfield, PA) for thin section
645 transmission electron microscopy (TEM) and thick section electron tomography (ET). TEM of
646 hundreds of cells per strain is used to quality control freezing, embedding, and staining for
647 tomography [61]. Tomographic samples are en bloc stained with 0.1% uranyl acetate and 0.25%
648 glutaraldehyde only, with no additional post staining as before [82]. 100 cells were surveyed before
649 at least 4 representative cells were selected to gather the tomography.
650
651 Thick sections were labeled with 15 nm fiducial gold on both sides and mapped on a Phillips
652 CM10 (TEM; Mahwah, NJ) at 80-kv and tilt-imaged with a Tecnai 30 (300kV FEI; Beaverton,
653 OR) with dual tilt series images collected from +60 to -60 degrees with 1 degree increment using
654 a Gatan US4000 4k x 4k CCD camera. Tilt-series were shot at 19,000 times magnification with a
655 0.6534 nm working pixel (binning 2) and repeated at a 90 degree rotation for dual-axis
656 tomography. Tomograms and models were constructed using IMOD software package [83].
657
658 MVB membrane models from dual-axis electron tomograms are manually assigned from the
659 inner leaflet every 4 nm and calculated using Imodmesh (3DMOD). We designated budding
660 profiles (BPs) by their negative curvature since the majority of endosome limiting membrane
661 curvature is positive, or spherical in shape. BP models are drawn from the 0° rim at the outer
662 leaflet, measured, and sorted by surface area using only BPs that have more than 750 nm^2 or
663 approximately half of the mean ILV surface [26]. ILVs are spherical and measured using sphere-
664 fitting models from the vesicle's outer leaflet (the inner leaflet of the MVB limiting membrane)
665 and ILV diameters are measured using these sphere models. Movies were made using IMOD and
666 QuickTime (Apple, Cupertino, CA). Data were analyzed and graphed using Prism 5 (GraphPad,
667 San Diego, CA).

Acknowledgements:
We would like to acknowledge Drs. Gina Razidlo and Jason Tan (Mayo Clinic, Rochester) for their inquiries and thoughtful discussions. SD, CT contributed to these studies as members of the Biochemistry and Molecular Biology Graduate Program and received financial support from the Mayo Clinic Graduate School of Biomedical Sciences.

Funding:
This research was supported, in whole or in part, by National Institutes of Health Grant R01 GM116826 (to D.J.K.), R01 GM065505 (to G.O.), R01 GM58202 (to R.C.P) and by a Fraternal Order of the Eagles postdoctoral fellowship (to B.A.D.). SED was supported by the National Science Foundation Graduate Research Fellowship under Grant No. (DGE-NSF-01-02). CT was supported by the Mayo Clinic Sydney Luckman Family Predoctoral Fellowship. JS was supported by the Mayo Clinic Summer Undergraduate Research Fellowship. The authors declare that they have no conflicts of interest with the contents of this article. The content is solely the responsibility of the authors and does not necessarily represent the official views of the National Institutes of Health. Any opinion, findings, and conclusions or recommendations expressed in this material are those of the authors(s) and do not necessarily reflect the views of the National Science Foundation.

Author Contributions: BD, IA and DJK conceived of the study. SD, BD, CT, and DJK designed and conducted the experiments along with JP, JS, NP, MW, and GO. DK, CT, BD and SD wrote the manuscript. All authors reviewed the results and approved the final version of the manuscript.

692 **Supplemental Figures:**

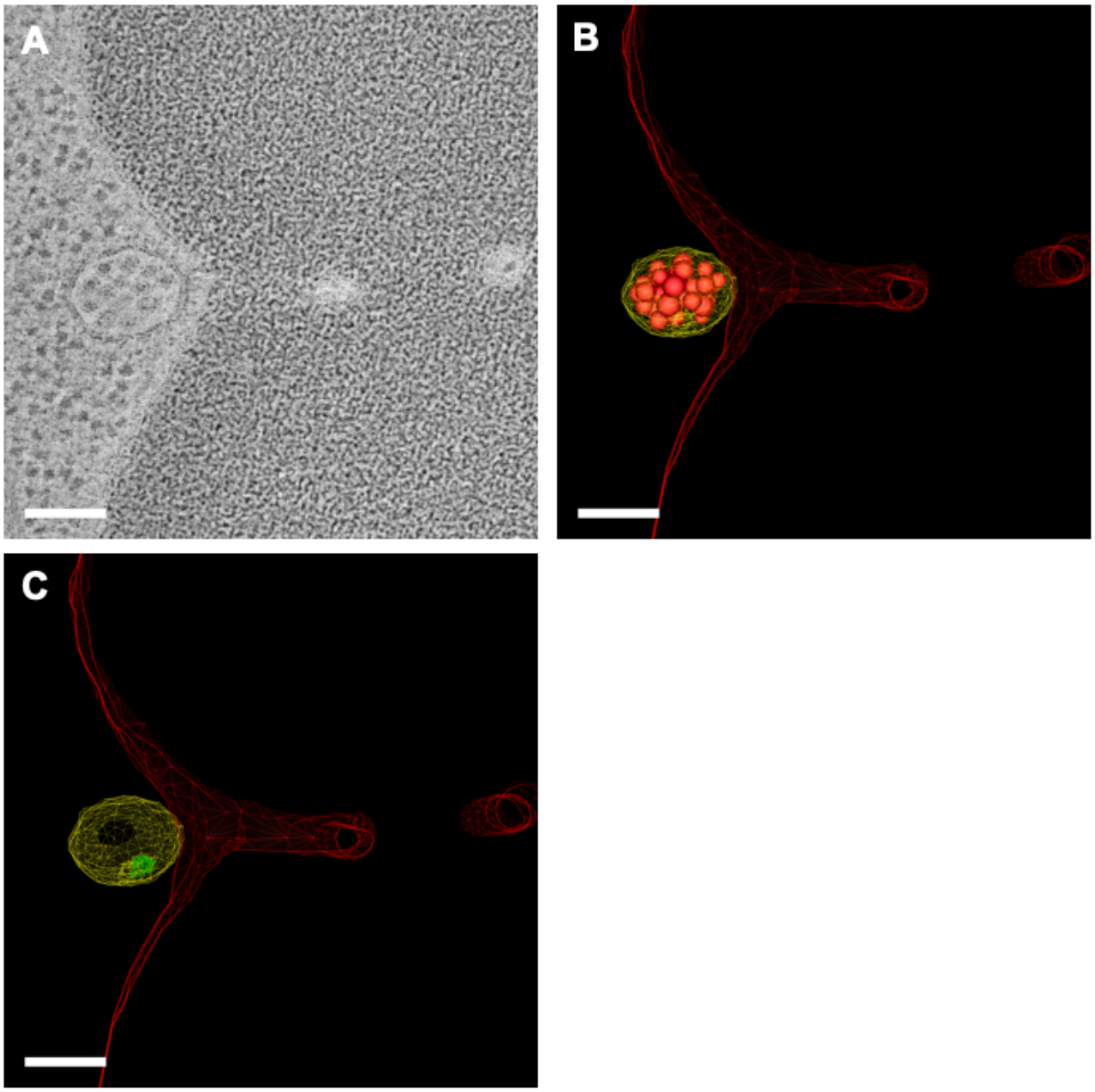

693

694 **Figure 1 Supplement 1. Electron tomography of WT cells expressing Bro1CTFΔUBD. (A)**
695 Representative electron micrograph of an MVB from WT cells expressing Bro1CTFΔUBD. **(B)**
696 3D reconstruction of the MVB from **(A)**. The MVB limiting membrane is labeled yellow and the
697 ILVs are highlighted in red. **(C)** 3D reconstruction of the MVB from **(A)**, without the ILVs. The
698 budding profile is highlighted in green. Scale bar = 100nm.

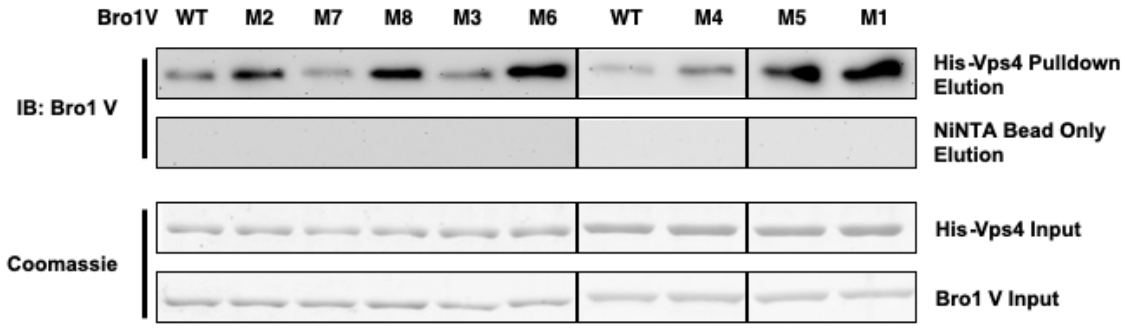

Figure 4 Supplement 1. Bro1 V domain mutants still bind Vps4. Immobilized His-Vps4 or Ni-NTA beads alone were incubated with Bro1V or Bro1V mutants and bound material was visualized by Western blotting with anti-Bro1 antiserum.

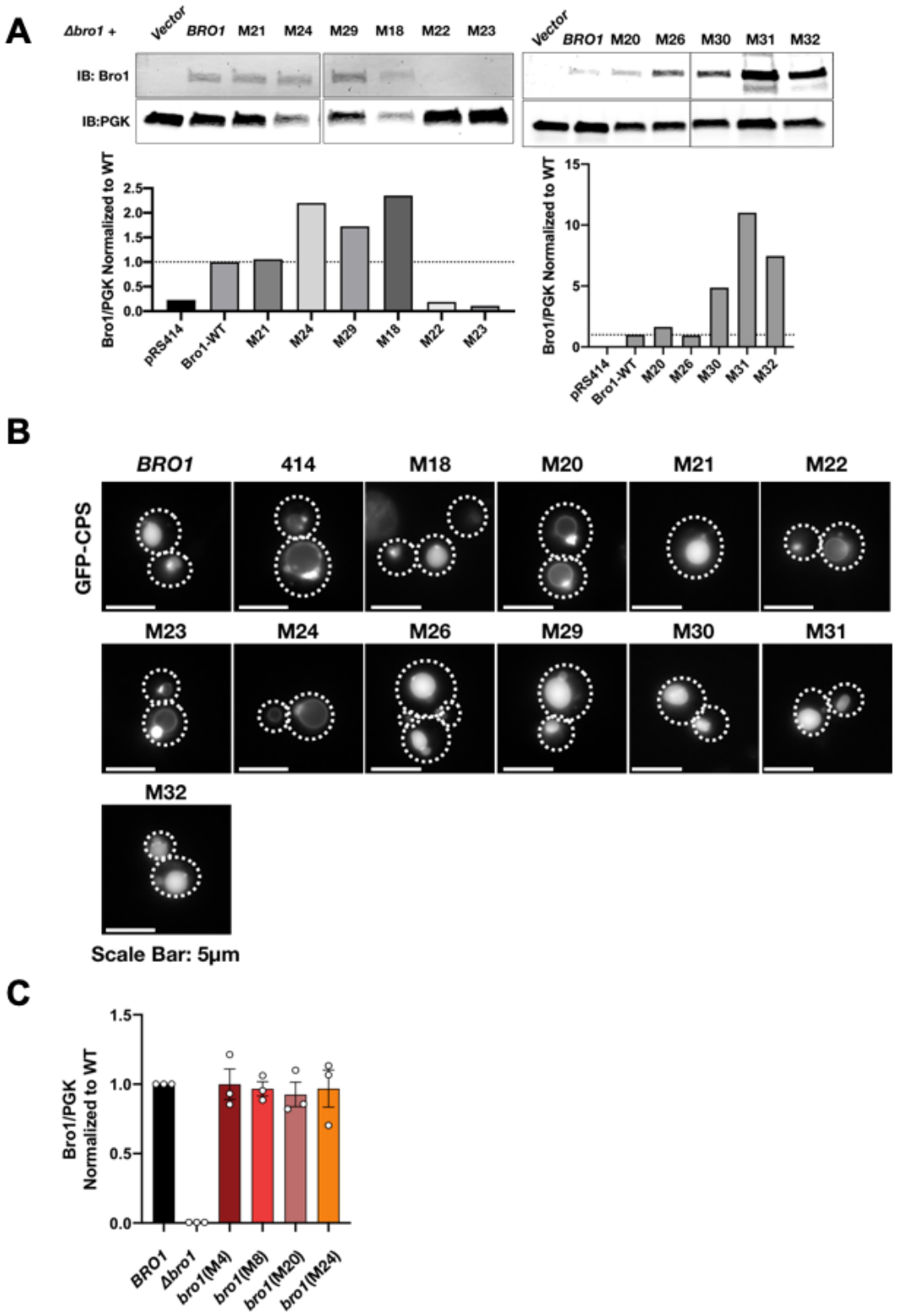

703

704 **Figure 5 Supplement 1. Evaluating the expression and the impact on cargo sorting of Bro1**
705 **V domain mutants. (A)** Western blot analysis of Bro1 and PGK expression level in *bro1*Δ

706 (GOY65) cells transformed with empty plasmid (vector), *BRO1*, or Bro1V mutants. **(B)** Live cell
707 fluorescence microcopy analysis of GFP-CPS sorting in GOY65 (*bro1*Δ) transformed with
708 empty plasmid (vector), *BRO1*, or Bro1V mutants. **(C)** Quantification of Western blot analysis of
709 Bro1 levels in *bro1*Δ cells transformed with empty plasmid (vector), *BRO1*, or mutants
710 *bro1*(M4), *bro1*(M8), *bro1*(M24). Error bars indicate mean ± S.E.M. Differences between WT
711 and mutant expression levels are not statistically significant.

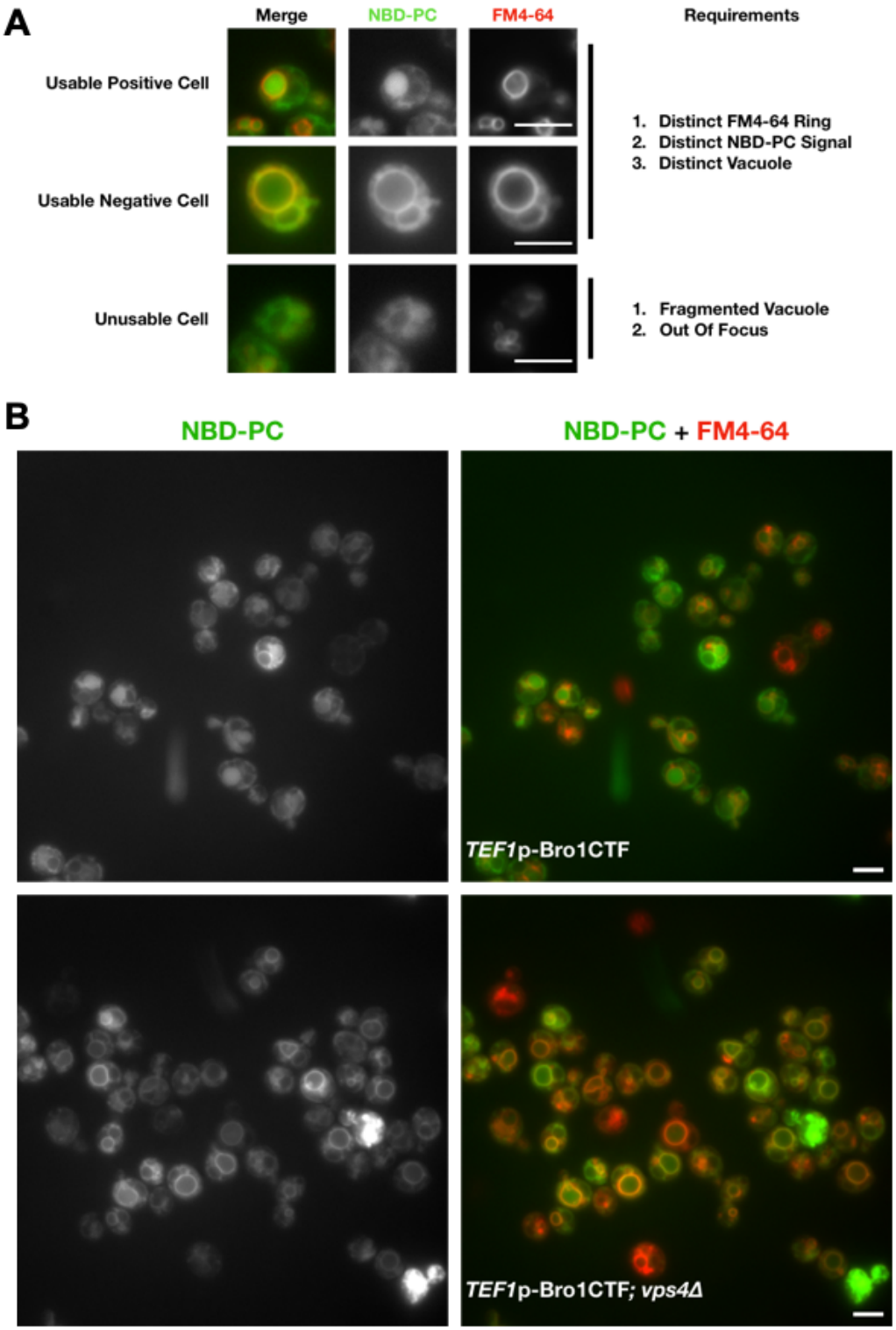

712

713 **Figure 9 Supplement 1. Representative images of cells stained with NBD-PC and FM4-64.**
714 This figure complements Figure 3. **(A)** Selection criteria for scoring positive NBD-PC cells. A
715 usable cell is defined by having (1) a distinct FM4-64 ring, (2) a distinct NBD-PC signal, and (3)

716 a distinct vacuole. An unusable cell is defined by having (1) a fragmented vacuole, and (2) out of
717 focus. A positive cell is defined by a diffuse NBD-PC signal while lacking a distinct ring on the
718 limiting membrane of the vacuole; while a negative cell is defined by the colocalization of NBD-
719 PC and FM4-64 on the limiting membrane of the vacuole. Scale = 5µm. **(B)** Representative
720 micrographs of *bro1*Δ*::TEF1*p-Bro1CTF (CTY2) and *vps4*Δ*::TRP1 bro1*Δ*::TEF1*p-Bro1CTF
721 (CTY5) cells stained with NBD-PC to label ILVs and FM4-64 to label vacuoles. Scale = 5µm.
722
723 **Figure 1 Supplement Movie 1. Tomogram of MVB in a WT cell.** MVBs in WT yeast are
724 roughly spherical membrane structures that contain smaller membrane-bound vesicles. This
725 video shows two WT MVBs that are adjacent to the vacuole (red mesh). The limiting endosomal
726 membrane is shown in yellow, and the intralumenal vesicles are in red. Scale bar = 100nm.
727
728 **Figure 1 Supplement Movie 2. Tomogram of MVB in a WT cell expressing**
729 **Bro1CTFΔUBD.** MVBs in a WT cell expressing Bro1CTFΔUBD exhibits WT MVB
730 morphology. This video shows one MVB next to the vacuole (red mesh). The limiting membrane
731 of the MVB is colored yellow and the intralumenal vesicles are in red. Intermediate budding
732 profiles are highlighted in green. Scale bar = 100nm.
733
734 **Figure 1 Supplement Movie 3. Tomogram of MVB in a *bro1*Δ cell.** *bro1*Δ cell has class E
735 compartments, which are flattened stacks of endosomal membranes that generally lack internal
736 vesicles. Cisternal class E compartment stacks are shown in different colors to differentiate
737 individual membranes. The vacuolar limiting membrane is labeled red. Scale bar = 100nm.
738
739 **Figure 1 Supplement Movie 4. Tomogram of MVB in a *bro1*Δ*::TEF1*p-Bro1CTF cell.**
740 MVBs in a *bro1*Δ*::TEF1*p-Bro1CTF cell exhibits WT MVB morphology. This video shows nine
741 MVBs that are adjacent to the vacuole (red mesh), while the limiting membrane of the MVB is
742 colored yellow and the intralumenal vesicles are in red. Intermediate budding profiles are
743 highlighted in green. Scale bar = 100nm.
744
745 **Figure 6 Supplement Movie 1. Tomogram of MVB in a *bro1*Δ cell expressing Bro1(M8).**
746 This tomogram depicts a single MVB adjacent to a vacuole (red mesh) from a *bro1*Δ cell
747 expressing Bro1(M8). The single MVB contains three budding intermediates (green), while its
748 limiting membrane is indicated by yellow and the intralumenal vesicles are labeled. Scale bar =
749 100nm.
750
751

752 **Supplemental Table 1. List of plasmids used in this study.**

Name	Description	Reference
pSD1	*S. cerevisiae* Bro1 V domain (Bro1V, aa 370-709) in pGST-parallel1	This study
pSD2	*S. cerevisiae* Bro1V L386R in pGST-parallel1 (M1)	This study
pSD3	*S. cerevisiae* Bro1V S414A, D415A in pGST-parallel1 (M2)	This study
pSD4	*S. cerevisiae* Bro1V S537A, L538A, L539A in pGST-parallel1 (M3)	This study
pSD5	*S. cerevisiae* Bro1V V505A, H508A, I512A in pGST-parallel1 (M4)	This study
pSD6	*S. cerevisiae* Bro1V F446A, E451A, F452A in pGST-parallel1 (M5)	This study
pSD7	*S. cerevisiae* Bro1V D454A, E457A, K461A in pGST-parallel1 (M6)	This study
pSD8	*S. cerevisiae* Bro1V V463A, L470A in pGST-parallel1 (M7)	This study
pSD9	*S. cerevisiae* Bro1V E686A, L691D in pGST-parallel1 (M8)	This study
pSD12	*BRO1* promoter driven *S. cerevisiae* Bro1 in pRS414 (WT)	This study
pSD13	*BRO1* promoter driven *S. cerevisiae* Bro1 S537A, L538A, L539A in pRS414 (M4)	This study
pSD14	*BRO1* promoter driven *S. cerevisiae* Bro1 V463A, L470A in pRS414 (M8)	This study
pCT2	*S. cerevisiae* Bro1V R570D in pGST-parallel1 (M18)	This study
pCT4	*S. cerevisiae* Bro1V T587D in pGST-parallel1 (M20)	This study
pCT5	*S. cerevisiae* Bro1V K611D in pGST-parallel1 (M21)	This study
pCT6	*S. cerevisiae* Bro1V A494D in pGST-parallel1 (M22)	This study
pCT7	*S. cerevisiae* Bro1V L501D in pGST-parallel1 (M23)	This study
pCT8	*S. cerevisiae* Bro1V K481D in pGST-parallel1 (M24)	This study
pCT10	*S. cerevisiae* Bro1V Y688D in pGST-parallel1 (M26)	This study
pCT13	*S. cerevisiae* Bro1V D585R in pGST-parallel1 (M29)	This study
pCT14	*S. cerevisiae* Bro1V D498R in pGST-parallel1 (M30)	This study
pCT15	*S. cerevisiae* Bro1V F687R in pGST-parallel1 (M31)	This study
pCT16	*S. cerevisiae* Bro1V Y688R in pGST-parallel1 (M32)	This study

pCT18	*BRO1* promoter driven *S. cerevisiae* Bro1 R570D in pRS414 (M18)	This study
pCT20	*BRO1* promoter driven *S. cerevisiae* Bro1 T587D in pRS414 (M20)	This study
pCT21	*BRO1* promoter driven *S. cerevisiae* Bro1 K611D in pRS414 (M21)	This study
pCT22	*BRO1* promoter driven *S. cerevisiae* Bro1 A494D in pRS414 (M22)	This study
pCT23	*BRO1* promoter driven *S. cerevisiae* Bro1 L501D in pRS414 (M23)	This study
pCT24	*BRO1* promoter driven *S. cerevisiae* Bro1 K481D in pRS414 (M24)	This study
pCT26	*BRO1* promoter driven *S. cerevisiae* Bro1 Y688D in pRS414 (M26)	This study
pCT29	*BRO1* promoter driven *S. cerevisiae* Bro1 D585R in pRS414 (M29)	This study
pCT30	*BRO1* promoter driven *S. cerevisiae* Bro1 D498R in pRS414 (M30)	This study
pCT31	*BRO1* promoter driven *S. cerevisiae* Bro1 F687R in pRS414 (M31)	This study
pCT32	*BRO1* promoter driven *S. cerevisiae* Bro1 Y688R in pRS414 (M32)	This study
pCT33	*S. cerevisiae* Bro1 V I377R in pGST-parallel1 ("UBD-Mut")	This study
pCT34	pRS413 with two silent mutations (D133D, D153D) in *HIS3* cassette	This study
pCT35	pCT34 *HIS3* Cassette (D133D, D153D) in pFA6a-HisMX6 (*TEF1* promoter Template Plasmid)	This study
pCT36	*TEF1* promoter driven *S. cerevisiae* Bro1V (aa370-709) in pCT35	This study
pCT37	*TEF1* promoter driven *S. cerevisiae* Bro1V (aa370-709) and 500bp 3'UTR in pCT35	This study
pRS413	Low copy yeast shuttle plasmid containing HIS marker	[99]
pFA6a-His3MX6	*A. gossypii TEF1* promoter driven *S. pombe HIS3* in pFA plasmid	[100]

pRS414	Low copy yeast shuttle plasmid containing TRP marker	[72]
pGO216	*BRO1* promoter driven Bro1 in pRS426	[26]
pMB54	Vps4 in pGST-parallel1	[42]
pET28-Vps4	Vps4 in pET28a	[43]
pGO642	*BRO1* promoter driven Bro1 CTF (aa 388-844) in pRS426	[81]
pGO187	*BRO1* promoter driven Bro1 in pRS416	[71]
GFP-Ste2	*STE2* promoter driven GFP-Ste2 in pRS426	[73]
pPL4146	*CUP1* promoter driven Mup1-GFP in pR315	[95]
pGO45	*CPS* promoter driven CPS-GFP in pRS426	[73]
Ub-GFP-CPS	*CPS* promoter driven Ub-CPS-GFP in pRS426	[88]
pMA24	*TDH3* promoter driven Cos1-GFP in pGDP416	[75]
pMA25	*TDH3* promoter driven Cos2-GFP in pGDP416	[75]
pMA27	*TDH3* promoter driven Cos5-GFP in pGDP416	[75]
pRS416 Sna3-GFP	*SNA3* promoter driven Sna3-GFP in pRS416	[91]
pGO89	*DAP2* promoter driven DPAP B-GFP in pRS426	[73]
DPAP-B-GFP	*DAP2* promoter driven DPAP B-GFP in pRS425	This Study
pPL4443	*S. castellii* Bro1V (aa 370-708) in pET151	[48]
pPL4981	*S. castellii* Bro1V I377R (aa 370-708) in pET151 (“UBD-Mut”)	[48]
pPL4672	Human HD-PTPV (aa 361-711) in pET151	[48]
pPL5293	T7 promoter driven WT mono-Ub in pET21a	This Study

753
754
755

756 **Supplemental Table 2. List of primers used in this study.**

Name	Sequence	Notes	Reference
V5Prime370NcoI	caaccatggatgtctatgaaaaggaaagtatttac	generating pCT34	This study
V3Prime710EcoRI	atatgaattcctactcggtctgctttgcaac	generating pCT34	This study
413 BglII-1 Mut Frd	cactttccagagcggtggtagacctttcgaacag	generating pCT35	This study
413 BglII-1 Mut Rev	taccaccgctctggaaagtgcctcatccaaag	generating pCT35	This study
413 BglII-2 Mut Frd	caaagggagaaagtaggagacctctcttgcgagatg	generating pCT35	This study
413 BglII-2 Mut Rev	tcctactttctccctttgcaaaccaagttcga	generating pCT35	This study
413 BglII-Intr primer 5’	ggtggtagatctcgttttaagagcttggtgagcgc	generating pCT36	This study
413 PacI-Intr primer 3’	ggtggtttaattaacgcatagatccgtcgagttcaagag	generating pCT36	This study
BRO3UTR5PrimerEcoRI	atatgaattcgcatttcttatttcttaattttattgtagc	generating pCT37	This study
BRO3UTR3PrimerSacI	atatccgcggcgaggatgatgacgattgg	generating pCT37	This study
Tef1 target BRO1 5’UTR	tatgaggagaggcctttttccaatccagcttctctgtgtcttttagcttaggtcaaataagtaaggtttcatggttgtttatgttcggatgtgatgtg	generating CTY1-4	This study
Tef1 target BRO1 3’-370	gtttcttcaacttgctttctcaacagcgtcgctttttcttctgagtaaatactttccttttcatagacatccatggttgtttatgttcggatgtgatgtg	generating CTY2	This study
Tef1 target BRO1 3’-388	ctgggtagatttgtaaattcgatgaaggaagaatattccaaatttgctgtctcagtttcttcaacttgcttcatggttgtttatgttcggatgtgatgtg	generating CTY3	This study
TEF1pBRO3UTRAmp3Prime	cggcgaggatgatgacgattgg	generating CTY4	This study

757
758
759

760 **Supplemental Table 3. List of yeast strains used in this study.**

Name	Description	Reference
SEY6210	MATα, *leu2-3,112 ura3-52 his3-Δ200 trp1-Δ901 lys2-801 suc2-Δ9*	[101]
SEY6210.1	MATa, *leu2-3,112 ura3-52 his3-Δ200 trp1-Δ901 lys2-801 suc2-Δ9*	[101]
MBY3	SEY6210; *vps4Δ::TRP1*	[18]
GOY65	SEY6210; *bro1Δ::HIS3*	[71]
MBY52	TVY615; *vps4Δ::TRP1 pep4Δ::LEU2 prb1Δ::LEU2*	[88]
EEY9	SEY6210; *snf7Δ::HIS3*	[15]
JPY403	SEY6210; *vps4Δ::TRP1 pep4Δ::LEU2 bro1Δ::HIS3*	This study
CTY1	SEY6210.1; *bro1Δ::HIS3-TEF1*p-*BRO1*	This study
CTY2	SEY6210.1; *bro1Δ::HIS3-TEF1*p-*bro1-Δ1* (encoding Bro1 aa370-844) "Bro1CTF"	This study
CTY3	SEY6210.1; *bro1Δ::HIS3-TEF1*p-*bro1-Δ2* (encoding Bro1 aa388-844) "Bro1CTFΔUBD"	This study
CTY4	SEY6210.1; *bro1Δ::HIS3-TEF1*p-*bro1-Δ3* (encoding Bro1 aa370-709) "Bro1V "	This study
CTY5	SEY6210.1; *vps4Δ::TRP1 bro1Δ::HIS3-TEF1*p-*bro1-Δ1* ("Bro1CTF")	This study

761

762

763 **Supplemental Table 4. List of mutations analyzed in this study.** Only mutations that were
764 expressed and exhibited defective ATPase stimulation or MVB cargo sorting were pursued.

ID	Mutation	ATPase Stimulation/MVB Cargo Sorting	Yeast Expression
M1	L386R	+	+
M2	S414A, D415A	+	+
M3	S537A, L538A, L539A	+	+
M4	V505A, H508A, I512A	-	+
M5	F446A, E451A, F452A	+	+
M6	D454A, E457A, K461A	+	+
M7	V463A, L470A	+	+
M8	E686A, L691D	-	+
M18	R570D	+	+
M20	T587D	-	+
M21	K611D	+	+
M22	A494D	-	-
M23	L501D	-	-
M24	K481D	-	+
M26	Y688D	+	+
M29	D585R	+	+
M30	D498R	+	+
M31	F687R	+	+
M32	Y688R	+	+
M33	I377R	+	+

765
766
767
768

References

1 Vietri, M., Radulovic, M. & Stenmark, H. The many functions of ESCRTs. *Nature Reviews Molecular Cell Biology* **21**, 25-42, doi:10.1038/s41580-019-0177-4 (2020).

2 Hanson, P. I. & Cashikar, A. Multivesicular Body Morphogenesis. *Annual Review of Cell and Developmental Biology* **28**, 337-362, doi:10.1146/annurev-cellbio-092910-154152 (2012).

3 Schmidt, O. & Teis, D. The ESCRT machinery. *Curr Biol* **22**, R116-120, doi:10.1016/j.cub.2012.01.028 (2012).

4 Piper, R. C. & Lehner, P. J. Endosomal transport via ubiquitination. *Trends in Cell Biology* **21**, 647-655, doi:10.1016/j.tcb.2011.08.007 (2011).

5 Adell, M. A. & Teis, D. Assembly and disassembly of the ESCRT-III membrane scission complex. *FEBS Lett* **585**, 3191-3196, doi:10.1016/j.febslet.2011.09.001 (2011).

6 Alonso, Y. A. M., Migliano, S. M. & Teis, D. ESCRT-III and Vps4: a dynamic multipurpose tool for membrane budding and scission. *FEBS J* **283**, 3288-3302, doi:10.1111/febs.13688 (2016).

7 Votteler, J. & Sundquist, W. I. Virus Budding and the ESCRT Pathway. *Cell Host Microbe* **14**, 232-241, doi:10.1016/j.chom.2013.08.012 (2013).

8 Christ, L., Raiborg, C., Wenzel, E. M., Campsteijn, C. & Stenmark, H. Cellular Functions and Molecular Mechanisms of the ESCRT Membrane-Scission Machinery. *Trends Biochem.Sci.* **42**, 42-56, doi:10.1016/j.tibs.2016.08.016 (2017).

9 Webster, Brant M., Colombi, P., Jäger, J. & Lusk, C. P. Surveillance of Nuclear Pore Complex Assembly by ESCRT-III/Vps4. *Cell* **159**, 388-401, doi:https://doi.org/10.1016/j.cell.2014.09.012 (2014).

10 Hurley, J. H. ESCRTs are everywhere. *The EMBO Journal* **34**, 2398-2407, doi:10.15252/embj.201592484 (2015).

11 Henne, W. M., Buchkovich, N. J., Zhao, Y. & Emr, S. D. The endosomal sorting complex ESCRT-II mediates the assembly and architecture of ESCRT-III helices. *Cell* **151**, 356-371, doi:10.1016/j.cell.2012.08.039 (2012).

12 Guizetti, J. *et al.* Cortical Constriction During Abscission Involves Helices of ESCRT-III–Dependent Filaments. *Science* **331**, 1616, doi:10.1126/science.1201847 (2011).

13 Teis, D., Saksena, S. & Emr, S. D. Ordered Assembly of the ESCRT-III Complex on Endosomes Is Required to Sequester Cargo during MVB Formation. *Developmental Cell* **15**, 578-589, doi:10.1016/j.devcel.2008.08.013 (2008).

14 Hanson, P. I., Roth, R., Lin, Y. & Heuser, J. E. Plasma membrane deformation by circular arrays of ESCRT-III protein filaments. *The Journal of Cell Biology* **180**, 389-402, doi:10.1083/jcb.200707031 (2008).

806 15 Babst, M., Katzmann, D. J., Estepa-Sabal, E. J., Meerloo, T. & Emr, S. D. Escrt-III: An
807 endosome-associated heterooligomeric protein complex required for mvb sorting.
808 *Developmental Cell* **3**, 271-282, doi:10.1016/S1534-5807(02)00220-4 (2002).
809 16 Davies, B. A. *et al.* Coordination of Substrate Binding and ATP Hydrolysis in Vps4-
810 Mediated ESCRT-III Disassembly. *Molecular Biology of the Cell* **21**, 3396-3408,
811 doi:10.1091/mbc.e10-06-0512 (2010).
812 17 Babst, M., Wendland, B., Estepa, E. J. & Emr, S. D. The Vps4p AAA ATPase regulates
813 membrane association of a Vps protein complex required for normal endosome function.
814 *The EMBO Journal* **17**, 2982-2993, doi:10.1093/emboj/17.11.2982 (1998).
815 18 Babst, M., Sato, T. K., Banta, L. M. & Emr, S. D. Endosomal transport function in yeast
816 requires a novel AAA-type ATPase, Vps4p. *The EMBO Journal* **16**, 1820-1831,
817 doi:10.1093/emboj/16.8.1820 (1997).
818 19 Adell, M. A. Y. *et al.* Recruitment dynamics of ESCRT-III and Vps4 to endosomes and
819 implications for reverse membrane budding. *Elife* **6**, doi:10.7554/eLife.31652 (2017).
820 20 Muzioł, T. *et al.* Structural Basis for Budding by the ESCRT-III Factor CHMP3.
821 *Developmental Cell* **10**, 821-830, doi:10.1016/j.devcel.2006.03.013 (2006).
822 21 Wollert, T. & Hurley, J. H. Molecular mechanism of multivesicular body biogenesis by
823 ESCRT complexes. *Nature* **464**, 864-869, doi:10.1038/nature08849 (2010).
824 22 Wollert, T., Wunder, C., Lippincott-Schwartz, J. & Hurley, J. H. Membrane scission by
825 the ESCRT-III complex. *Nature* **458**, 172-177, doi:10.1038/nature07836 (2009).
826 23 Nickerson, D. P., West, M., Henry, R. & Odorizzi, G. Regulators of Vps4 ATPase
827 Activity at Endosomes Differentially Influence the Size and Rate of Formation of
828 Intralumenal Vesicles. *Molecular Biology of the Cell* **21**, 1023-1032,
829 doi:10.1091/mbc.e09-09-0776 (2010).
830 24 Nickerson, D. P., West, M. & Odorizzi, G. Did2 coordinates Vps4-mediated dissociation
831 of ESCRT-III from endosomes. *The Journal of Cell Biology* **175**, 715,
832 doi:10.1083/jcb.200606113 (2006).
833 25 Saksena, S., Wahlman, J., Teis, D., Johnson, A. E. & Emr, S. D. Functional reconstitution
834 of ESCRT-III assembly and disassembly. *Cell* **136**, 97-109,
835 doi:10.1016/j.cell.2008.11.013 (2009).
836 26 Wemmer, M. *et al.* Bro1 binding to Snf7 regulates ESCRT-III membrane scission
837 activity in yeast. *J Cell Biol* **192**, 295-306, doi:10.1083/jcb.201007018 (2011).
838 27 Adell, M. A. Y. *et al.* Coordinated binding of Vps4 to ESCRT-III drives membrane neck
839 constriction during MVB vesicle formation. *The Journal of Cell Biology* **205**, 33,
840 doi:10.1083/jcb.201310114 (2014).

28 Pfitzner, A.-K., Mercier, V. & Roux, A. Vps4 triggers sequential subunit exchange in ESCRT-III polymers that drives membrane constriction and fission. *bioRxiv*, 718080, doi:10.1101/718080 (2019).

29 Maity, S. *et al.* VPS4 triggers constriction and cleavage of ESCRT-III helical filaments. *Science Advances* **5**, eaau7198, doi:10.1126/sciadv.aau7198 (2019).

30 Caillat, C. *et al.* Asymmetric ring structure of Vps4 required for ESCRT-III disassembly. *Nature Communications* **6**, 8781, doi:10.1038/ncomms9781 (2015).

31 Ghazi-Tabatabai, S. *et al.* Structure and Disassembly of Filaments Formed by the ESCRT-III Subunit Vps24. *Structure* **16**, 1345-1356, doi:10.1016/j.str.2008.06.010 (2008).

32 Lata, S. *et al.* Helical Structures of ESCRT-III Are Disassembled by VPS4. *Science* **321**, 1354, doi:10.1126/science.1161070 (2008).

33 Guo, E. Z. & Xu, Z. Distinct Mechanisms of Recognizing Endosomal Sorting Complex Required for Transport III (ESCRT-III) Protein IST1 by Different Microtubule Interacting and Trafficking (MIT) Domains. *Journal of Biological Chemistry* **290**, 8396-8408, doi:10.1074/jbc.M114.607903 (2015).

34 Kieffer, C. *et al.* Two Distinct Modes of ESCRT-III Recognition Are Required for VPS4 Functions in Lysosomal Protein Targeting and HIV-1 Budding. *Developmental Cell* **15**, 62-73, doi:10.1016/j.devcel.2008.05.014 (2008).

35 Merrill, S. A. & Hanson, P. I. Activation of human VPS4A by ESCRT-III proteins reveals ability of substrates to relieve enzyme autoinhibition. *J Biol Chem* **285**, 35428-35438, doi:10.1074/jbc.M110.126318 (2010).

36 Obita, T. *et al.* Structural basis for selective recognition of ESCRT-III by the AAA ATPase Vps4. *Nature* **449**, 735-739, doi:10.1038/nature06171 (2007).

37 Scott, A. *et al.* Structure and ESCRT-III protein interactions of the MIT domain of human VPS4A. *Proc. Natl. Acad. Sci. U. S. A.* **102**, 13813, doi:10.1073/pnas.0502165102 (2005).

38 Shim, S., Kimpler, L. A. & Hanson, P. I. Structure/function analysis of four core ESCRT-III proteins reveals common regulatory role for extreme C-terminal domain. *Traffic* **8**, 1068-1079, doi:10.1111/j.1600-0854.2007.00584.x (2007).

39 Stuchell-Brereton, M. D. *et al.* ESCRT-III recognition by VPS4 ATPases. *Nature* **449**, 740-744, doi:10.1038/nature06172 (2007).

40 Shestakova, A., Curtiss, M., Davies, B. A., Katzmann, D. J. & Babst, M. The Linker Region Plays a Regulatory Role in Assembly and Activity of the Vps4 AAA ATPase. *Journal of Biological Chemistry* **288**, 26810-26819, doi:10.1074/jbc.M113.497032 (2013).

877 41 Azmi, I. *et al.* Recycling of ESCRTs by the AAA-ATPase Vps4 is regulated by a
878 conserved VSL region in Vta1. *J Cell Biol* **172**, 705-717, doi:10.1083/jcb.200508166
879 (2006).
880 42 Azmi, I. F. *et al.* ESCRT-III Family Members Stimulate Vps4 ATPase Activity Directly
881 or via Vta1. *Developmental Cell* **14**, 50-61,
882 doi:https://doi.org/10.1016/j.devcel.2007.10.021 (2008).
883 43 Davies, B. A. *et al.* Vps4 stimulatory element of the cofactor Vta1 contacts the ATPase
884 Vps4 α7 and α9 to stimulate ATP hydrolysis. *The Journal of biological chemistry* **289**,
885 28707-28718, doi:10.1074/jbc.M114.580696 (2014).
886 44 Han, H. *et al.* Binding of Substrates to the Central Pore of the Vps4 ATPase Is
887 Autoinhibited by the Microtubule Interacting and Trafficking (MIT) Domain and
888 Activated by MIT Interacting Motifs (MIMs). *Journal of Biological Chemistry* **290**,
889 13490-13499, doi:10.1074/jbc.M115.642355 (2015).
890 45 Luhtala, N. & Odorizzi, G. Bro1 coordinates deubiquitination in the multivesicular body
891 pathway by recruiting Doa4 to endosomes. *The Journal of Cell Biology* **166**, 717,
892 doi:10.1083/jcb.200403139 (2004).
893 46 Nikko, E. & André, B. Split-Ubiquitin Two-Hybrid Assay To Analyze Protein-Protein
894 Interactions at the Endosome: Application to Saccharomyces cerevisiae Bro1 Interacting
895 with ESCRT Complexes, the Doa4 Ubiquitin Hydrolase, and the Rsp5 Ubiquitin Ligase.
896 *Eukaryotic Cell* **6**, 1266, doi:10.1128/EC.00024-07 (2007).
897 47 Norgan, A. P. *et al.* Relief of autoinhibition enhances Vta1 activation of Vps4 via the
898 Vps4 stimulatory element. *J Biol Chem* **288**, 26147-26156,
899 doi:10.1074/jbc.M113.494112 (2013).
900 48 Pashkova, N. *et al.* The Yeast Alix Homolog Bro1 Functions as a Ubiquitin Receptor for
901 Protein Sorting into Multivesicular Endosomes. *Developmental Cell* **25**, 520-533,
902 doi:10.1016/j.devcel.2013.04.007 (2013).
903 49 Richter, C., West, M. & Odorizzi, G. Dual mechanisms specify Doa4-mediated
904 deubiquitination at multivesicular bodies. *The EMBO Journal* **26**, 2454-2464,
905 doi:10.1038/sj.emboj.7601692 (2007).
906 50 Shestakova, A. *et al.* Assembly of the AAA ATPase Vps4 on ESCRT-III. *Mol Biol Cell*
907 **21**, 1059-1071, doi:10.1091/mbc.E09-07-0572 (2010).
908 51 Tan, J., Davies, B. A., Payne, J. A., Benson, L. M. & Katzmann, D. J. Conformational
909 Changes in the Endosomal Sorting Complex Required for the Transport III Subunit Ist1
910 Lead to Distinct Modes of ATPase Vps4 Regulation. *J Biol Chem* **290**, 30053-30065,
911 doi:10.1074/jbc.M115.665604 (2015).

912 52 Shim, S., Merrill, S. A. & Hanson, P. I. Novel interactions of ESCRT-III with LIP5 and
913 VPS4 and their implications for ESCRT-III disassembly. *Mol Biol Cell* **19**, 2661-2672,
914 doi:10.1091/mbc.E07-12-1263 (2008).
915 53 Dowlatshahi, Dara P. *et al.* ALIX Is a Lys63-Specific Polyubiquitin Binding Protein that
916 Functions in Retrovirus Budding. *Developmental Cell* **23**, 1247-1254,
917 doi:https://doi.org/10.1016/j.devcel.2012.10.023 (2012).
918 54 Fisher, R. D. *et al.* Structural and Biochemical Studies of ALIX/AIP1 and Its Role in
919 Retrovirus Budding. *Cell* **128**, 841-852, doi:10.1016/j.cell.2007.01.035 (2007).
920 55 Keren-Kaplan, T. *et al.* Structure-based in silico identification of ubiquitin-binding
921 domains provides insights into the ALIX-V:ubiquitin complex and retrovirus budding.
922 *The EMBO journal* **32**, 538-551, doi:10.1038/emboj.2013.4 (2013).
923 56 Sun, S. *et al.* ALG-2 activates the MVB sorting function of ALIX through relieving its
924 intramolecular interaction. *Cell Discovery* **1**, 15018, doi:10.1038/celldisc.2015.18 (2015).
925 57 Ali, N. *et al.* Recruitment of UBPY and ESCRT Exchange Drive HD-PTP-Dependent
926 Sorting of EGFR to the MVB. *Current Biology* **23**, 453-461,
927 doi:10.1016/j.cub.2013.02.033 (2013).
928 58 von Schwedler, U. K. *et al.* The Protein Network of HIV Budding. *Cell* **114**, 701-713,
929 doi:10.1016/S0092-8674(03)00714-1 (2003).
930 59 Ichioka, F. *et al.* HD-PTP and Alix share some membrane-traffic related proteins that
931 interact with their Bro1 domains or proline-rich regions. *Archives of Biochemistry and*
932 *Biophysics* **457**, 142-149, doi:https://doi.org/10.1016/j.abb.2006.11.008 (2007).
933 60 Lee, J. *et al.* Structural Study of the HD-PTP Bro1 Domain in a Complex with the Core
934 Region of STAM2, a Subunit of ESCRT-0. *PLOS ONE* **11**, e0149113,
935 doi:10.1371/journal.pone.0149113 (2016).
936 61 Richter, C. M., West, M. & Odorizzi, G. Doa4 function in ILV budding is restricted
937 through its interaction with the Vps20 subunit of ESCRT-III. *J Cell Sci* **126**, 1881-1890,
938 doi:10.1242/jcs.122499 (2013).
939 62 Strack, B., Calistri, A., Craig, S., Popova, E. & Göttlinger, H. G. AIP1/ALIX Is a
940 Binding Partner for HIV-1 p6 and EIAV p9 Functioning in Virus Budding. *Cell* **114**, 689-
941 699, doi:https://doi.org/10.1016/S0092-8674(03)00653-6 (2003).
942 63 Bowers, K. *et al.* Protein–Protein Interactions of ESCRT Complexes in the Yeast
943 Saccharomyces cerevisiae. *Traffic* **5**, 194-210, doi:10.1111/j.1600-0854.2004.00169.x
944 (2004).
945 64 Katoh, K. *et al.* The ALG-2-interacting Protein Alix Associates with CHMP4b, a Human
946 Homologue of Yeast Snf7 That Is Involved in Multivesicular Body Sorting. *Journal of*
947 *Biological Chemistry* **278**, 39104-39113, doi:10.1074/jbc.M301604200 (2003).

948 65 Kim, J. *et al.* Structural Basis for Endosomal Targeting by the Bro1 Domain.
949 *Developmental Cell* **8**, 937-947, doi:10.1016/j.devcel.2005.04.001 (2005).
950 66 McCullough, J., Fisher, R. D., Whitby, F. G., Sundquist, W. I. & Hill, C. P. ALIX-
951 CHMP4 interactions in the human ESCRT pathway. *Proceedings of the National*
952 *Academy of Sciences* **105**, 7687, doi:10.1073/pnas.0801567105 (2008).
953 67 Parkinson, Michael D. J. *et al.* A non-canonical ESCRT pathway, including histidine
954 domain phosphotyrosine phosphatase (HD-PTP), is used for down-regulation of virally
955 ubiquitinated MHC class I. *Biochemical Journal* **471**, 79-88, doi:10.1042/BJ20150336
956 (2015).
957 68 Sette, P., Nagashima, K., Piper, R. C. & Bouamr, F. Ubiquitin conjugation to Gag is
958 essential for ESCRT-mediated HIV-1 budding. *Retrovirology* **10**, 79, doi:10.1186/1742-
959 4690-10-79 (2013).
960 69 Vajjhala, P. R., Catchpoole, E., Nguyen, C. H., Kistler, C. & Munn, A. L. Vps4 regulates
961 a subset of protein interactions at the multivesicular endosome. *The FEBS Journal* **274**,
962 1894-1907, doi:10.1111/j.1742-4658.2007.05736.x (2007).
963 70 Sheffield, P., Garrard, S. & Derewenda, Z. Overcoming expression and purification
964 problems of RhoGDI using a family of "parallel" expression vectors. *Protein Expr Purif*
965 **15**, 34-39, doi:10.1006/prep.1998.1003 (1999).
966 71 Odorizzi, G., Katzmann, D. J., Babst, M., Audhya, A. & Emr, S. D. Bro1 is an
967 endosome-associated protein that functions in the MVB pathway in Saccharomyces
968 cerevisiae. *J Cell Sci* **116**, 1893-1903, doi:10.1242/jcs.00395 (2003).
969 72 Simons, R. W., Houman, F. & Kleckner, N. Improved single and multicopy lac-based
970 cloning vectors for protein and operon fusions. *Gene* **53**, 85-96, doi:10.1016/0378-
971 1119(87)90095-3 (1987).
972 73 Odorizzi, G., Babst, M. & Emr, S. D. Fab1p PtdIns(3)P 5-Kinase Function Essential for
973 Protein Sorting in the Multivesicular Body. *Cell* **95**, 847-858, doi:10.1016/S0092-
974 8674(00)81707-9 (1998).
975 74 Sundd, M., Iverson, N., Ibarra-Molero, B., Sanchez-Ruiz, J. M. & Robertson, A. D.
976 Electrostatic interactions in ubiquitin: stabilization of carboxylates by lysine amino
977 groups. *Biochemistry* **41**, 7586-7596, doi:10.1021/bi025571d (2002).
978 75 MacDonald, C. *et al.* A family of tetraspans organizes cargo for sorting into
979 multivesicular bodies. *Dev Cell* **33**, 328-342, doi:10.1016/j.devcel.2015.03.007 (2015).
980 76 Schindelin, J. *et al.* Fiji: an open-source platform for biological-image analysis. *Nature*
981 *Methods* **9**, 676-682, doi:10.1038/nmeth.2019 (2012).
982 77 Dimaano, C., Jones, C. B., Hanono, A., Curtiss, M. & Babst, M. Ist1 Regulates Vps4
983 Localization and Assembly. *Molecular Biology of the Cell* **19**, 465-474,
984 doi:10.1091/mbc.e07-08-0747 (2007).

78 Pettersen, E. F. *et al.* UCSF Chimera--a visualization system for exploratory research and analysis. *J Comput Chem* **25**, 1605-1612, doi:10.1002/jcc.20084 (2004).
79 Schrödinger, L. The PyMOL Molecular Graphics System, Version 2.0.
80 Buysse, D., Pfitzner, A.-K., West, M., Roux, A. & Odorizzi, G. The ubiquitin hydrolase Doa4 directly binds Snf7 to inhibit recruitment of ESCRT-III remodeling factors in <em>S. cerevisiae</em&gt. *Journal of Cell Science* **133**, jcs241455, doi:10.1242/jcs.241455 (2020).
81 Johnson, N., West, M. & Odorizzi, G. Regulation of yeast ESCRT-III membrane scission activity by the Doa4 ubiquitin hydrolase. *Mol Biol Cell* **28**, 661-672, doi:10.1091/mbc.E16-11-0761 (2017).
82 Giddings, T. H. Freeze-substitution protocols for improved visualization of membranes in high-pressure frozen samples. *Journal of Microscopy* **212**, 53-61, doi:10.1046/j.1365-2818.2003.01228.x (2003).
83 Kremer, J. R., Mastronarde, D. N. & McIntosh, J. R. Computer Visualization of Three-Dimensional Image Data Using IMOD. *Journal of Structural Biology* **116**, 71-76, doi:https://doi.org/10.1006/jsbi.1996.0013 (1996).
84 Kimura, Y. *et al.* Conserved Mode of Interaction between Yeast Bro1 Family V Domains and YP(X)nL Motif-Containing Target Proteins. *Eukaryot Cell* **14**, 976-982, doi:10.1128/ec.00091-15 (2015).
85 Lee, S., Joshi, A., Nagashima, K., Freed, E. O. & Hurley, J. H. Structural basis for viral late-domain binding to Alix. *Nature Structural &Amp; Molecular Biology* **14**, 194, doi:10.1038/nsmb1203 (2007).
86 Tang, S. *et al.* ESCRT-III activation by parallel action of ESCRT-I/II and ESCRT-0/Bro1 during MVB biogenesis. *eLife* **5**, e15507, doi:10.7554/eLife.15507 (2016).
87 Katzmann, D. J., Babst, M. & Emr, S. D. Ubiquitin-Dependent Sorting into the Multivesicular Body Pathway Requires the Function of a Conserved Endosomal Protein Sorting Complex, ESCRT-I. *Cell* **106**, 145-155, doi:10.1016/S0092-8674(01)00434-2 (2001).
88 Katzmann, D. J., Sarkar, S., Chu, T., Audhya, A. & Emr, S. D. Multivesicular Body Sorting: Ubiquitin Ligase Rsp5 Is Required for the Modification and Sorting of Carboxypeptidase S. *Molecular Biology of the Cell* **15**, 468-480, doi:10.1091/mbc.e03-07-0473 (2003).
89 MacDonald, C., Stringer, D. K. & Piper, R. C. Sna3 Is an Rsp5 Adaptor Protein that Relies on Ubiquitination for Its MVB Sorting. *Traffic* **13**, 586-598, doi:10.1111/j.1600-0854.2011.01326.x (2012).

1020 90 Oestreich, A. J., Davies, B. A., Payne, J. A. & Katzmann, D. J. Mvb12 Is a Novel
1021 Member of ESCRT-I Involved in Cargo Selection by the Multivesicular Body Pathway.
1022 *Molecular Biology of the Cell* **18**, 646-657, doi:10.1091/mbc.e06-07-0601 (2006).
1023 91 Reggiori, F. & Pelham, H. R. B. Sorting of proteins into multivesicular bodies: ubiquitin-
1024 dependent and -independent targeting. *The EMBO Journal* **20**, 5176-5186,
1025 doi:10.1093/emboj/20.18.5176 (2001).
1026 92 Bilodeau, P. S., Urbanowski, J. L., Winistorfer, S. C. & Piper, R. C. The Vps27p–Hse1p
1027 complex binds ubiquitin and mediates endosomal protein sorting. *Nature Cell Biology* **4**,
1028 534, doi:10.1038/ncb815 (2002).
1029 93 Hanson, P. K., Grant, A. M. & Nichols, J. W. NBD-labeled phosphatidylcholine enters
1030 the yeast vacuole via the pre-vacuolar compartment. *Journal of Cell Science* **115**, 2725
1031 (2002).
1032 94 Shields, S. B. *et al.* ESCRT ubiquitin-binding domains function cooperatively during
1033 MVB cargo sorting. *The Journal of cell biology* **185**, 213-224,
1034 doi:10.1083/jcb.200811130 (2009).
1035 95 Stringer, D. K. & Piper, R. C. A single ubiquitin is sufficient for cargo protein entry into
1036 MVBs in the absence of ESCRT ubiquitination. *The Journal of Cell Biology* **192**, 229,
1037 doi:10.1083/jcb.201008121 (2011).
1038 96 MacDonald, C., Buchkovich, N. J., Stringer, D. K., Emr, S. D. & Piper, R. C. Cargo
1039 ubiquitination is essential for multivesicular body intralumenal vesicle formation. *EMBO*
1040 *reports* **13**, 331, doi:10.1038/embor.2012.18 (2012).
1041 97 Swaney, D. L. *et al.* Global analysis of phosphorylation and ubiquitylation cross-talk in
1042 protein degradation. *Nature Methods* **10**, 676-682, doi:10.1038/nmeth.2519 (2013).
1043 98 Larios, J., Mercier, V., Roux, A. & Gruenberg, J. ALIX- and ESCRT-III–dependent
1044 sorting of tetraspanins to exosomes. *J. Cell Biol.* **219**, doi:10.1083/jcb.201904113 (2020).
1045 99 Sikorski, R. S. & Hieter, P. A system of shuttle vectors and yeast host strains designed
1046 for efficient manipulation of DNA in Saccharomyces cerevisiae. *Genetics* **122**, 19-27
1047 (1989).
1048 100 Longtine, M. S. *et al.* Additional modules for versatile and economical PCR-based gene
1049 deletion and modification in Saccharomyces cerevisiae. *Yeast* **14**, 953-961,
1050 doi:10.1002/(SICI)1097-0061(199807)14:10<953::AID-YEA293>3.0.CO;2-U (1998).
1051 101 Robinson, J. S., Klionsky, D. J., Banta, L. M. & Emr, S. D. Protein sorting in
1052 Saccharomyces cerevisiae: isolation of mutants defective in the delivery and processing
1053 of multiple vacuolar hydrolases. *Molecular and Cellular Biology* **8**, 4936,
1054 doi:10.1128/MCB.8.11.4936 (1988).